NEUROPHYSIOLOGY

Asprosin promotes feeding through SK channel–dependent activation of AgRP neurons

Bing Feng[1]†, Hesong Liu[2]†, Ila Mishra[3]†, Clemens Duerrschmid[4], Peiyu Gao[1], Pingwen Xu[5]*, Chunmei Wang[2]*, Yanlin He[1]*

Asprosin, a recently identified adipokine, activates agouti-related peptide (AgRP) neurons in the arcuate nucleus of the hypothalamus (ARH) via binding to protein tyrosine phosphatase receptor δ (Ptprd) to increase food intake. However, the intracellular mechanisms responsible for asprosin/Ptprd-mediated activation of AgRP^{ARH} neurons remain unknown. Here, we demonstrate that the small-conductance calcium-activated potassium (SK) channel is required for the stimulatory effects of asprosin/Ptprd on AgRP^{ARH} neurons. Specifically, we found that deficiency or elevation of circulating asprosin increased or decreased the SK current in AgRP^{ARH} neurons, respectively. AgRP^{ARH}-specific deletion of SK3 (an SK channel subtype highly expressed in AgRP^{ARH} neurons) blocked asprosin-induced AgRP^{ARH} activation and overeating. Furthermore, pharmacological blockade, genetic knockdown, or knockout of Ptprd abolished asprosin's effects on the SK current and AgRP^{ARH} neuronal activity. Therefore, our results demonstrated an essential asprosin-Ptprd-SK3 mechanism in asprosin-induced AgRP^{ARH} activation and hyperphagia, which is a potential therapeutic target for the treatment of obesity.

INTRODUCTION

Asprosin, a recently identified fasting-induced orexigenic hormone, was first found by A. Chopra in 2016 through studying a rare genetic disease called neonatal progeroid syndrome (NPS) (*1*). Using whole-exome sequencing, Chopra and colleagues (*1*) identified the responsible genetic mutations, which prevent patients with NPS from generating a previously unknown hormone, asprosin. Patients with NPS have significantly lower levels of asprosin in the circulation compared to age- and sex-matched control subjects, associated with hypophagia, extremely low body mass index (BMI), and high insulin sensitivity (*2*), suggesting a potential metabolic role of asprosin.

Subsequently, to further study NPS, a transgenic mouse model with the same loss-of-function mutation in one allele of the asprosin-encoded gene, fibrillin 1(*Fbn1*$^{NPS/+}$), was generated. Similar to those observed in human patients with NPS, *Fbn1*$^{NPS/+}$ mutation results in decreased circulating asprosin, which is associated with hypophagia, leanness, and insulin sensitivity (*1*–*5*). Conversely, replenishing active asprosin in vivo to *Fbn1*$^{NPS/+}$ mice rescues these phenotypes (*2*). These animal studies provide direct evidence to support the vital role of asprosin in energy balance and glucose homeostasis. Notably, it has been shown that circulating asprosin can cross the blood-brain barrier, and fasting increases the levels of asprosin in the cerebrospinal fluid (CSF) (*2*). Mechanistically, we found that asprosin activates the agouti-related peptide (AgRP)–releasing neurons in the arcuate nucleus of the hypothalamus (AgRP^{ARH}) to promote appetite (*2*). However, the intracellular mechanism by which asprosin activates the AgRP^{ARH} neuronal activity is still not fully understood.

In 2019, three years after the discovery of asprosin, Li *et al.* (*6*) first identified an olfactory G protein–coupled receptor, *OR4M1* (*Olfr734* is the mouse ortholog), as the hepatic asprosin receptor responsible for asprosin-mediated hepatic glucose release. More recently, protein tyrosine phosphatase receptor δ (Ptprd), a membrane-bound phosphatase receptor, was identified as the orexigenic asprosin receptor in AgRP^{ARH} neurons (*7*). Ptprd does not contribute to asprosin-mediated hepatic glucose release, and Olfr734 is not involved in asprosin-mediated orexigenic, suggesting that asprosin uses two distinct receptors for its core functions (*7*). The essential role of Ptprd in appetite regulation has been demonstrated by several studies using transgenic mice. For example, both male and female mice with congenital global deletion of Ptprd (*Ptprd*$^{-/-}$) were much leaner and ate significantly less than their wild-type (WT) littermates. Consistently, specific deletion of Ptprd in AgRP^{ARH} neurons, either constitutively or in adulthood, protects animals from diet-induced obesity, suggesting potential therapeutic value.

The small-conductance calcium-activated potassium (SK) channel is a subfamily of Ca^{2+}-activated K^+ channels (*8*–*10*). The opening of SK channels allows potassium outflux, which is believed to constitute a large portion of the afterhyperpolarization (*11*). The SK channel family consists of four members, SK1, SK2, SK3, and SK4, widely expressed in many different tissues (*10*–*13*). SK3 (encoded by the *Kcnn3* gene) is abundantly expressed in the ARH and regulates proopiomelanocortin (POMC) activity and energy homeostasis (*10*, *14*), while the levels of other isoforms (SK1, SK2, and SK4) in the ARH are minimal (*15*, *16*). We and others reported that SK3 mRNA levels in AgRP/neuropeptide Y (NPY) neurons markedly decline after 24 hours of food deprivation and that pharmacological inhibition of SK currents can activate AgRP/NPY neurons (*16*, *17*). We previously reported that food deprivation suppresses SK3 expression in AgRP^{ARH} neurons, and the decreased SK3-mediated currents contribute to the fasting-

[1]Pennington Biomedical Research Center, Louisiana State University, Baton Rouge, LA, USA. [2]USDA-ARS Children's Nutrition Research Center, Department of Pediatrics, Baylor College of Medicine, Houston, TX, USA. [3]Harrington Discovery Institute, Cleveland, OH, USA. [4]Department of Molecular and Cellular Biology, Baylor College of Medicine, Houston, TX, USA. [5]Division of Endocrinology, Diabetes and Metabolism, Department of Medicine, The University of Illinois at Chicago, Chicago, IL, USA.
*Corresponding author. Email: pingwenx@uic.edu (P.X.); chunmeiw@bcm.edu (C. W.); yanlin.he@pbrc.edu (Y.H.)
†These authors contributed equally to this work.

induced activation of AgRP^{ARH} neurons. Selective knockout (KO) of SK3 from AgRP^{ARH} neurons increased sensitivity to diet-induced obesity, which is associated with chronic hyperphagia and reduced energy expenditure in mice (*17*). Together, SK3 expressed by AgRP^{ARH} neurons plays an important role in regulating food intake and body weight balance. In this current follow-up study of asprosin, we found that asprosin significantly inhibits SK currents via the Ptprd signaling in AgRP^{ARH} neurons. Thus, we hypothesize that asprosin regulates the AgRP^{ARH} neuronal firing activity by targeting the SK3 ion channel via Ptprd signaling.

The current study used pharmacologic and genetic mouse models with asprosin deficiency or surplus to investigate asprosin's effects on SK current and AgRP^{ARH} neuronal activity. Mice with SK3 selectively deleted from AgRP^{ARH} neurons were further used to examine the roles of SK3 in the stimulatory effects of asprosin on AgRP^{ARH} neurons and food intake. Last, we pharmacologically blocked Ptprd signaling or selectively knocked down/out Ptprd in AgRP^{ARH} neurons to explore the requirement of Ptprd for asprosin-mediated effects on SK current and AgRP^{ARH} neuronal activity.

RESULTS

Asprosin deficiency and surplus regulate SK current and activity of AgRP^{ARH} neurons

We previously reported that asprosin activates AgRP^{ARH} neurons to promote food intake after fasting (*2*). To identify the intracellular mechanism by which asprosin activates AgRP^{ARH} neurons, we crossed *Fbn1*$^{NPS/+}$ mice [a mouse strain carrying a mutated *Fbn1* allele that produces symptoms mimicking those of human patients with NPS (*2*)] with *AgRP-Cre/Rosa26-LSL-tdTOMATO* mice (this mouse strain has all AgRP neurons labeled with tdTOMATO reporter) to generate *Fbn1*$^{NPS/+}$*/AgRP-Cre/Rosa26-LSL-tdTOMATO* mice and control WT/*AgRP-Cre/Rosa26-LSL-tdTOMATO* mice (Fig. 1A). We then electrophysiologically characterized AgRP^{ARH} neurons from mice with normal (WT) or diminished (*Fbn1*$^{NPS/+}$) plasma asprosin under fed or fasted conditions (Fig. 1B). Our results indicated that the SK currents in AgRP^{ARH} neurons were increased in asprosin-deficient mice compared to their control littermates under both fed and fasted conditions (Fig. 1, C and D). Notably, compared to the fed condition, fasting significantly reduced the SK currents in WT control mice but not in the asprosin-deficient mice (Fig. 1D), suggesting that asprosin is necessary for the inhibitory effects of fasting on SK currents. Consistently, both action potential (AP) firing frequency and resting membrane potential of AgRP^{ARH} neurons were significantly reduced in asprosin-deficient mice under fed conditions (Fig. 1, E to G), indicating a baseline hyperpolarization. Fasting-induced increases in firing frequency and resting membrane potential of AgRP^{ARH} neurons were blocked by asprosin depletion (Fig. 1, E to G), indicating impaired natural dynamics of AgRP^{ARH} neuronal activity. Together, we conclude that asprosin is necessary for the fasting-induced inhibitory effect on the SK current and that asprosin is necessary for baseline activity and fasting-induced activation of AgRP^{ARH} neurons.

To further confirm whether asprosin directly inhibits SK currents in AgRP^{ARH} neurons, we incubated the AgRP^{ARH} neurons with a cocktail of synaptic blockers [1 μM tetrodotoxin (TTX), 30 μM 6-cyano-7-nitroquinoxaline-2,3-dione, 30 μM D-(-)-2-Amino-5-phosphonopentanoic acid (D-AP5), and 50 μM bicuculline] (*2*, *18*, *19*) to block the synaptic input from their upstream neurons. The SK current amplitude in AgRP^{ARH} neurons under fed condition did not show a significant difference with or without synaptic blockers (Fig. 1D and fig. S1B). In the presence of the synaptic blockers, asprosin still inhibited the SK currents and depolarized the resting membrane potential in AgRP^{ARH} neurons (fig. S1, A to E). These data indicate that asprosin directly inhibits SK currents and activates AgRP^{ARH} neurons.

To investigate the in vivo effects of asprosin, we generated an asprosin overexpression mouse model by tail vein injection of adeno-associated virus 8 (AAV8) encoding human cleaved asprosin [with an interleukin-2 (IL-2) signal peptide to promote secretion] as we described previously (Fig. 2A) (*7*). Two, 4, 6, and 8 weeks after virus injection, the mice were euthanized during the fed condition in the early mornings, and the SK current and neuronal firing activity of the AgRP^{ARH} neurons were recorded. Opposite to the observations from asprosin-deficient mice, we found that asprosin overexpression decreased the SK current and increased the firing frequency and depolarized resting membrane potential of AgRP^{ARH} neurons at 4, 6, and 8 weeks after virus injection, respectively (Fig. 2, B to D). Notably, these electrophysiological changes were associated with increased circulating asprosin (fig. S2A), body weight gain, hyperphagia, and glucose intolerance (Fig. 2, E to I). Eight weeks after virus injection, asprosin overexpression decreased the protein levels of the SK3 channel but not Ptprd, an orexigenic asprosin receptor (*7*), in AgRP^{ARH} neurons (fig. S2, B to E). These data exclude the potential counterregulatory response at the level of Ptprd. The decrease in SK3 protein is consistent with our previous observations that food deprivation suppresses SK3 expression in AgRP/NPY neurons (*17*). Considering the potential role of asprosin in the regulatory effects of food deprivation on AgRP neurons, the decreased SK3 protein is presumed to implicate the inhibitory effects of chronic asprosin action on SK3 expression. Together, prolonged increases in circulating asprosin inhibit SK current in AgRP^{ARH} neurons, which is associated with a corresponding rise in AgRP^{ARH} neuronal activity, hyperphagia, body weight gain, and glucose intolerance.

SK current and AgRP^{ARH} neuronal activity can be modulated in both directions via pharmacologic asprosin manipulation

Patients with NPS are known to have low levels of asprosin in the circulation, potentially contributing to their hypophagia and extremely low BMI (*2*, *20*–*23*). *Fbn1*$^{NPS/+}$ mice engineered to harbor the NPS mutation faithfully mimic all these features and provide a model to test the potential for treatment/rescue with asprosin replenishment. Here, we explored this hypothesis, specifically focusing on the SK current and AgRP^{ARH} neuronal activity. First, we ex vivo recorded the responses of AgRP^{ARH} neurons to the treatment of recombinant asprosin (1-hour incubation) or an irrelevant control protein [green fluorescent protein (GFP)] in brain slices from WT control and *Fbn1*$^{NPS/+}$ mice (Fig. 3A). Consistent with our previous observation (Fig. 1, C to G), AgRP^{ARH} neurons from *Fbn1*$^{NPS/+}$ mice showed an increase in the SK current and a decrease in firing frequency and resting membrane potential (Fig. 3, B to D) compared with these neurons from control mice. Notably, recombinant asprosin treatment restored the SK current, resting membrane potential, and activity of AgRP^{ARH} neuron to near WT control levels in *Fbn1*$^{NPS/+}$ mice (Fig. 3, B to D), suggesting a causal role for asprosin deficiency in the observed elevated SK

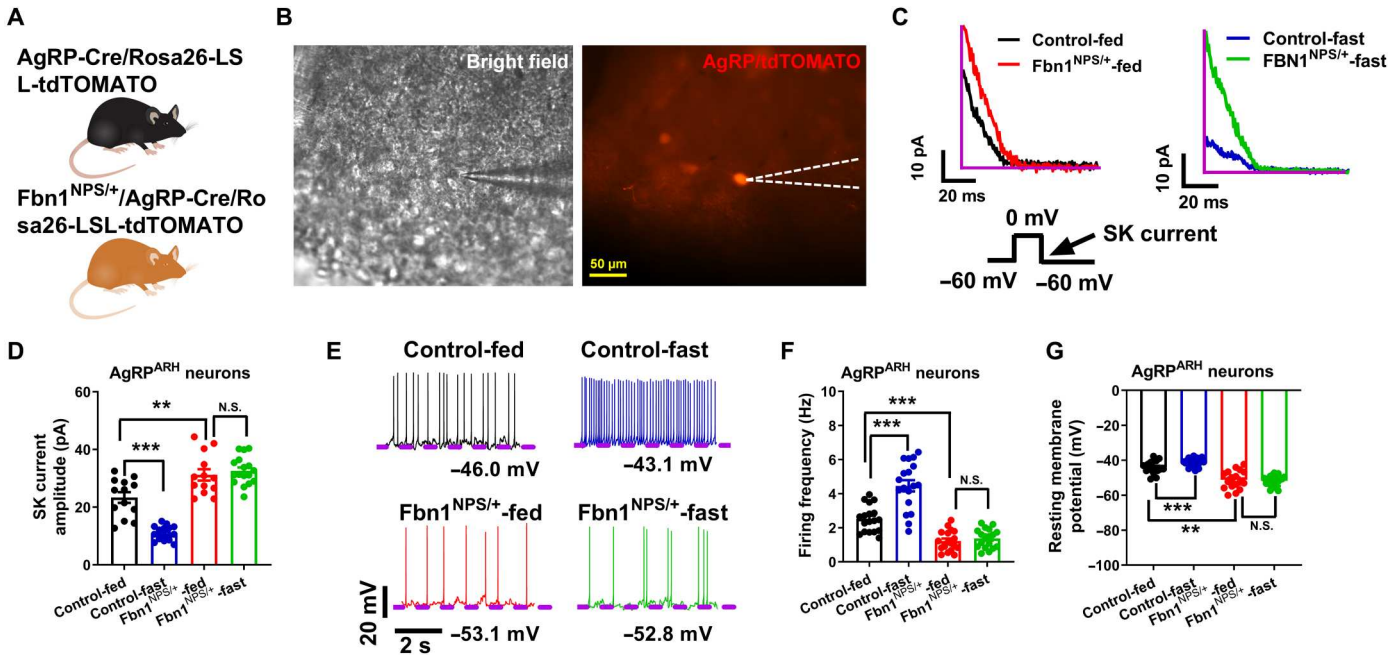

Fig. 1. Asprosin deficiency increases SK current and inhibits AgRP^{ARH} neurons. (**A**) Schematic of *AgRP-Cre/Rosa26-LSL-tdTOMATO* and *Fbn1$^{NPS/+}$/AgRP-Cre/Rosa26-LSL-tdTOMATO* mouse models used for electrophysiology recordings. (**B**) A representative tdTOMATO-positive AgRP neuron under whole-cell patch-clamp recording. Scale bar, 50 μm. (**C**) Top: representative SK current traces. Bottom: A published voltage protocol to detect the SK current in AgRP neurons. (**D**) Data analysis of SK current amplitude in AgRP^{ARH} neurons (n = 14 from three different animals in each group) from the control or *Fbn1$^{NPS/+}$* mice. N.S., not significant. (**E**) Representative AP traces in the AgRP^{ARH} neurons recorded from the control or *Fbn1$^{NPS/+}$* mice. (**F**) Data analysis of AP firing frequency and (**G**) resting membrane potential in AgRP^{ARH} neurons (n = 18 from three different animals in each group) from the control or *Fbn1$^{NPS/+}$* mice. Data are presented as means ± SEM with individual datapoints. $^{**}P < 0.01$ and $^{***}P < 0.001$ by two-tailed t test (D, F, and G).

current in *Fbn1$^{NPS/+}$* mice. Next, to test the in vivo effect of recombinant asprosin, we intraperitoneally injected immunoglobulin G (IgG) or recombinant asprosin in the *Fbn1$^{NPS/+}$* mice. The following morning, the brain sections containing AgRP^{ARH} neurons were collected for the electrophysiology recording (Fig. 3E). In vivo systemically replenishing asprosin in *Fbn1$^{NPS/+}$* mice significantly reduced the SK current and increased the firing frequency and resting membrane potential of AgRP^{ARH} neurons compared to the control IgG injected in the *Fbn1$^{NPS/+}$* mice (Fig. 3, E to H). These results indicate a potential role of AgRP^{ARH}/SK signaling in the therapeutic beneficial metabolic effects of asprosin in patients with NPS.

In the opposite direction, obese patients have been shown to have high levels of asprosin in the circulation, associated with hyperphagia and body weight gain (*4*, *24*–*31*). On the basis of these observations, it is also promising to use an asprosin-neutralizing antibody to sequester asprosin-mediated orexigenic effects immunologically. Next, we tested whether up- or down-regulation of plasma asprosin in WT control mice can produce corresponding changes in SK current and AgRP^{ARH} neuronal activity. Specifically, we intraperitoneally injected WT mice with recombinant asprosin, an anti-asprosin-neutralizing monoclonal antibody (mAb), or IgG (Fig. 3I). The asprosin-neutralizing antibody can bind to the active asprosin protein and reduce the circulation levels of asprosin (*2*, *32*), and the IgG is an irrelevant antibody that served as a control for both treatments. We found that up-regulation of plasma asprosin inhibited the SK current and increased the AgRP^{ARH} neuronal activity (Fig. 3, J to L). Conversely, an asprosin-neutralizing mAb increased the SK current and inhibited AgRP^{ARH} neuronal activity (Fig. 3, J to L) compared to the control IgG–injected mice. These data indicate exquisite control of SK current and AgRP^{ARH} neuronal activity by asprosin in both directions.

SK3 is required for the stimulatory effects of asprosin on AgRP^{ARH} neurons and food intake

To directly test the requirement of SK current for asprosin-mediated AgRP^{ARH} neuron activation, we used a whole-cell patch-clamp to record the responses of AgRP^{ARH} neurons to asprosin in the presence of an SK channel blocker (apamin) or an SK channel opener (*N*-cyclohexyl-2-(3,5-dimethylpyrazol-1-yl)-6-methylpyrimidin-4-amine, CyPPA) in ex vivo brain slices of WT mice (Fig. 4A). Consistently, we found that asprosin puff treatment alone decreased SK current and activated AgRP^{ARH} neurons. Afterward, the AgRP^{ARH} neurons were bath applied with apamin or CyPPA for 4 min. As expected, apamin significantly inhibited SK current and activated AgRP neurons, while CyPPA did the opposite. Subsequently, we performed a similar puff treatment of asprosin in the presence of apamin or CyppA in the bath solution. We found that pharmacological inhibition (apamin) or activation (CyPPA) of the SK channel abolished the stimulatory effects of asprosin on the firing frequency and resting membrane potential of AgRP^{ARH} neurons. After we washed out apamin or CyPPA, these asprosin-induced stimulations were restored in AgRP neurons (Fig. 4, B to G, and fig. S3, A and B). We speculate that the unresponsiveness of AgRP^{ARH} neurons to asprosin in the presence of CyPPA or apamin is presumed to implicate the mode of interaction between asprosin and CyPPA or apamin. As a classic positive gating modulator of SK channels,

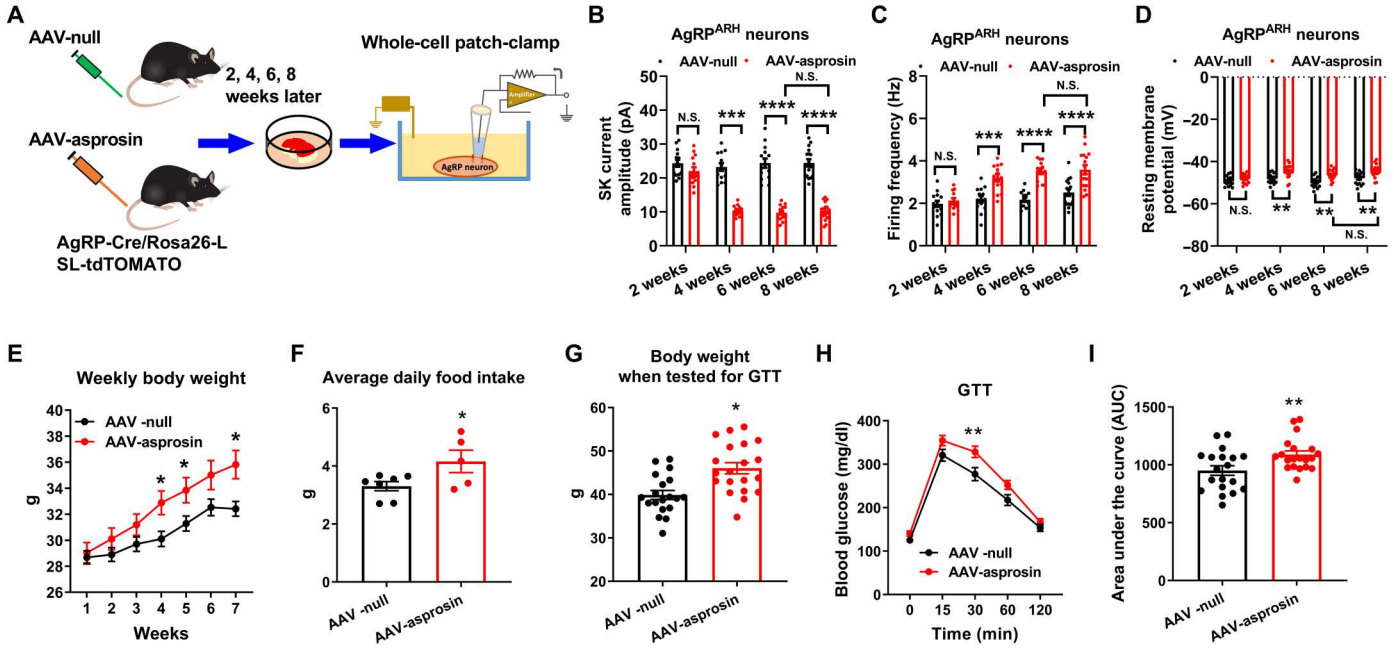

Fig. 2. Asprosin surplus decreases SK current, activates AgRP^{ARH} neurons, and promotes feeding behavior. (**A**) Schematic of AAV-null and AAV-asprosin overexpression virus injected in *AgRP-Cre/Rosa26-LSL-tdTOMATO* mice. (**B**) Data analysis of SK current amplitude, (**C**) AP firing frequency, and (**D**) resting membrane potential in AgRP^{ARH} neurons (n = 16 from three different animals in each group) after the mice received AAV-null or AAV-asprosin for different weeks (n = 13 or 16 from three different mice in each group). (**E**) Weekly body weight from the AAV-null–injected (n = 19) or AAV-asprosin–injected (n = 20) mice. (**F**) Average daily food intake measurements from AAV-null–injected (n = 7) or AAV-asprosin–injected mice (n = 6). (**G**) Body weight of AAV-null–injected (n = 19) and AAV-asprosin–injected (n = 20) mice after 8 weeks before the glucose tolerance test (GTT). (**H**) Blood glucose and (**I**) area under the curve in the GTT test of AAV-null (n = 19) and AAV-asprosin mice (n = 20). Data are presented as means ± SEM with individual datapoints. *P < 0.05, **P < 0.01, ***P < 0.001, and ****P < 0.0001 by two-way ANOVA analysis followed by post hoc Sidak tests (B to E and H) or by unpaired two-sample t test (F, G, and I).

the stimulatory effects of CyPPA likely override the inhibitory effects induced by asprosin on SK current. This is consistent with a previous report that the actions of CyPPA dominate the effects of a coapplied negative gating modulator, NS8593 (*33*). Conversely, as a potent SK channel blocker, apamin possibly suppresses SK current to a minimal level that no longer responds to asprosin's inhibition. Results from both directions suggest that inhibition of the SK channel is required for asprosin-mediated AgRP^{ARH} neuron activation.

To test this hypothesis in a genetic context, we recorded the responses of AgRP^{ARH} neurons to asprosin in mice with AgRP^{ARH} neuron–specific deletion of the SK3 channel (SK3^{AgRP} KO), the primary subtype of the SK channel expressed in hypothalamic AgRP^{ARH} neurons (Fig. 4H) (*16*, *17*). Consistent with our previous report (*17*), SK3^{AgRP} KO resulted in the depletion of SK3 protein (fig. S3, C and D), decreased SK current, depolarized resting membrane potential, and increased amplified firing frequency in AgRP^{ARH} neurons (Fig. 4, I to K). When SK3 was knocked out from AgRP^{ARH} neurons, incubation of asprosin for 1 hour in the bath solution failed to change the SK current and neuronal firing activity when compared to GFP treatment (Fig. 4, I to K). SK3^{AgRP} KO blocked the inhibitory effects of asprosin-neutralizing mAb on food intake (Fig. 4, L and M). Notably, ex vivo treatment of ghrelin, another well-known orexigenic hormone activating AgRP^{ARH} neurons (*34*–*36*), increased the firing frequency of AgRP^{ARH} neurons in both WT and SK3^{AgRP} KO mice without changing SK current (fig. S4, A to D). Thus, despite a high baseline level of AgRP^{ARH} neuronal activity upon SK3 deletion, AgRP^{ARH} neurons remain capable of further activation in response to a different orexigenic agent. These data suggest that the lack of response to asprosin upon SK3 deletion is independent of the high baseline AgRP^{ARH} neuronal activity resulting from the loss of SK3. Together, these results indicate that inhibition of the SK3 channel is required for asprosin-mediated AgRP^{ARH} neuron activation and appetite stimulation.

Asprosin inhibits SK current via Ptprd expressed by AgRP^{ARH} neurons

To test whether Ptprd, an asprosin receptor expressed by AgRP^{ARH} neurons, mediates asprosin's inhibitory effects on SK current, we electrophysiologically recorded the responses of AgRP^{ARH} neurons to asprosin in brain slices preincubated with 7-butoxy illudalic acid analog (7-BIA) (10 μM; 10 min of preincubation), a selective Ptprd inhibitor (Fig. 5A). We found that pharmacologically blocking Ptprd abolished asprosin-induced inhibition of the SK current and stimulation of AgRP^{ARH} neuronal activity (Fig. 5, B to D). Consistent with these ex vivo observations, we found that intraperitoneal injection of 7-BIA in the male C57BL/6 mice under the fed condition reduced dark- and fast-induced food intake in mice (Fig. 5, E to G).

As a second strategy, to avoid potential nonspecific impacts of pharmacologic Ptprd inhibition, AgRP^{ARH} neuron–specific *Ptprd* knockdown (KD) was accomplished genetically in adult mice. For this, Agrp-Cre mice received a bilateral stereotaxic injection of two

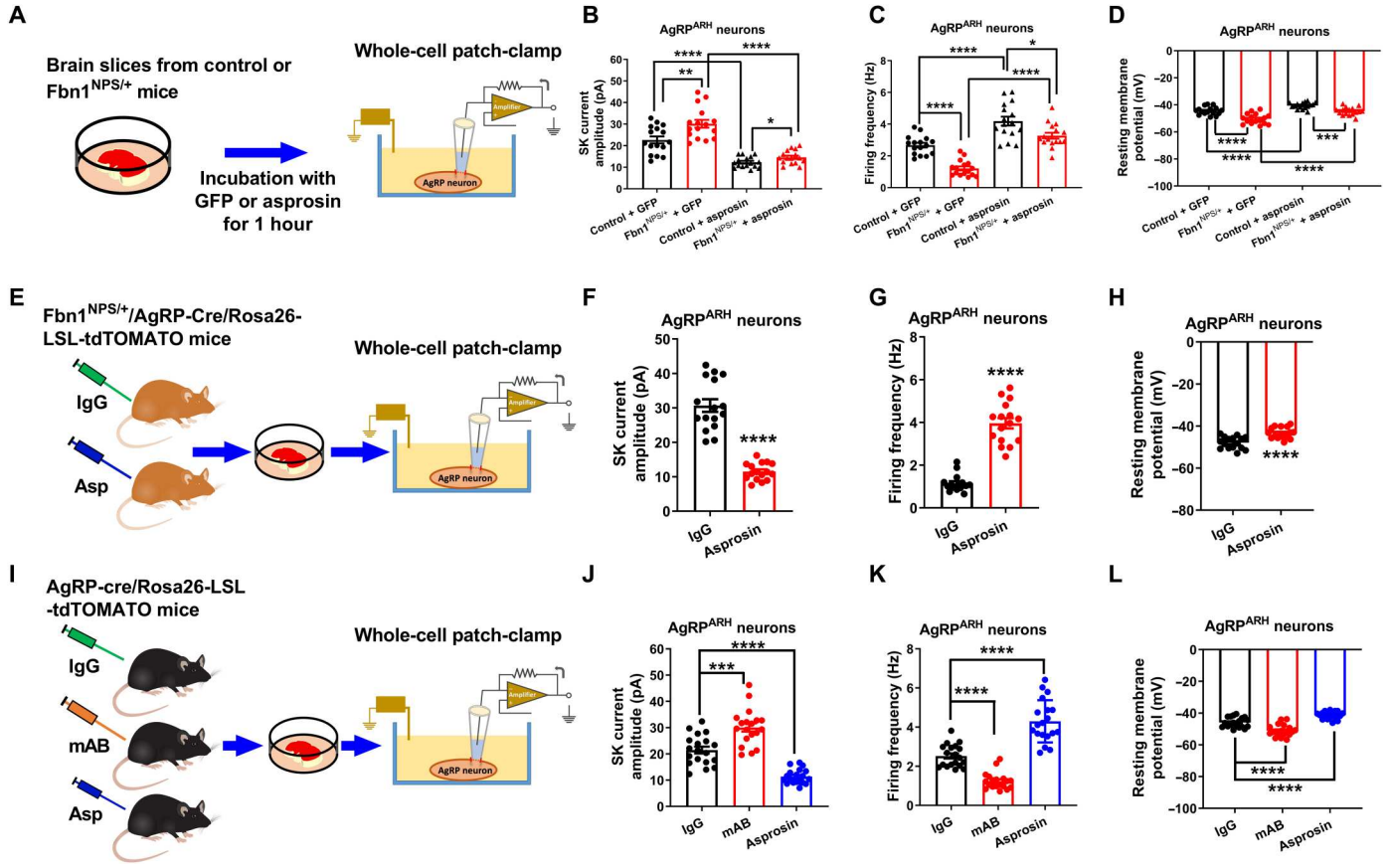

Fig. 3. SK current and AgRP^{ARH} neuronal activity can be modulated in both directions via pharmacologic asprosin manipulation. (**A**) Schematic of brain slices incubated with GFP or asprosin (1 hour) used for electrophysiology recordings from the *AgRP-Cre/Rosa26-LSL-tdTOMATO* (control) and *Fbn1$^{NPS/+}$/AgRP-Cre/Rosa26-LSL-tdTOMATO* (Fbn1$^{NPS/+}$) mouse models. (**B**) Data analysis of SK current amplitude, (**C**) AP firing frequency, and (**D**) resting membrane potential in AgRP^{ARH} neurons (n = 16 from three different animals in each group) from the control or Fbn1$^{NPS/+}$ mice. (**E**) Schematic of IgG or asprosin (Asp) injection in the *Fbn1$^{NPS/+}$/AgRP-Cre/Rosa26-LSL-tdTOMATO* mouse used for electrophysiology recordings. (**F**) Data analysis of SK current amplitude, (**G**) AP firing frequency, and (**H**) resting membrane potential in AgRP^{ARH} neurons (n = 16 from three different animals in each group). (**I**) Schematic of IgG, mAb, or asprosin (Asp) injection in the *AgRP-Cre/Rosa26-LSL-tdTOMATO* mouse used for electrophysiology recordings. (**J**) Data analysis of SK current amplitude, (**K**) AP firing frequency, and (**L**) resting membrane potential in AgRP^{ARH} neurons (n = 19 from three different animals in each group). Data are presented as means ± SEM with individual datapoints. *P < 0.05, **P < 0.01, ***P < 0.001, and ****P < 0.0001 by unpaired two-sample t test (B to D, F to H, and J to L).

AAV8 viruses in the ARH (*7*). The first AAV expressed a *Ptprd*-specific small guide RNA (sgRNA) and a Cre-dependent GFP protein, while the second AAV expressed a Cre-inducible cas9. As a result, *Ptprd* was knocked down with the expression of both sgRNA and Cas9 only in AgRP^{ARH} neurons. Control mice received the same sgRNA as experimental mice; however, the Cre-inducible cas9 was replaced with Cre-inducible mCherry (fig. S5A). This approach of knocking down *Ptprd* from AgRP neurons was previously validated in our 2022 publication (*7*). Four weeks after virus injection, we electrophysiologically recorded the response of green (GFP, Ptprd^{AgRP} KD)− or red (mCherry, control)−positive neurons in the ARH to the treatment of asprosin in brain slices (fig. S5B). We found that asprosin inhibited the SK current and stimulated AgRP^{ARH} neuronal activity in control mice (fig. S5, C to E), as we previously observed in WT mice. Conversely, all asprosin-induced regulatory effects were abolished in Ptprd^{AgRP} KD mice (fig. S5, C to E). These data indicate that Ptprd is necessary for asprosin's regulatory effects on SK current and activity of AgRP^{ARH} neurons.

Although *Ptprd*-sgRNA/cas9 effectively knocks down the expression of *Ptprd* (*7*), there is still a certain percentage of *Ptprd* expression in the AgRP^{ARH} neurons. To further target these neurons, we crossed *Ptprd$^{f/f}$* [*Ptprd* tm2c(KOMP)Wtsi] (*7*) mice with *AgRP-Cre/Rosa26-LSL-tdTOMATO* mice to generate a mouse model with *Ptprd* selectively deleted from the AgRP^{ARH} neuron (Ptprd^{AgRP} KO) (Fig. 6A). We used an anti-Ptprd antibody to validate that Ptprd was selectively knocked out only in AgRP^{ARH} neurons (fig. S6, A and B). Our electrophysiology data indicated that, when Ptprd was knocked out from AgRP^{ARH} neurons, 30 nM asprosin puff treatment failed to inhibit SK current, activate AgRP^{ARH} neuronal firing activity, or depolarize the resting membrane potential (Fig. 6, B to F). We previously showed that asprosin/Ptprd signaling modulates the firing activity of AgRP neurons via the adenosine 3′,5′-monophosphate (cAMP)–dependent protein kinase (PKA) pathway (*2*, *32*). To further test whether asprosin inhibits SK current via the Ptprd/PKA signal pathway, we recorded asprosin's effects on SK current and firing activity after pharmacologically blocking PKA by bath incubation of 1 μM PKI (a potent, heat-stable, and specific PKA

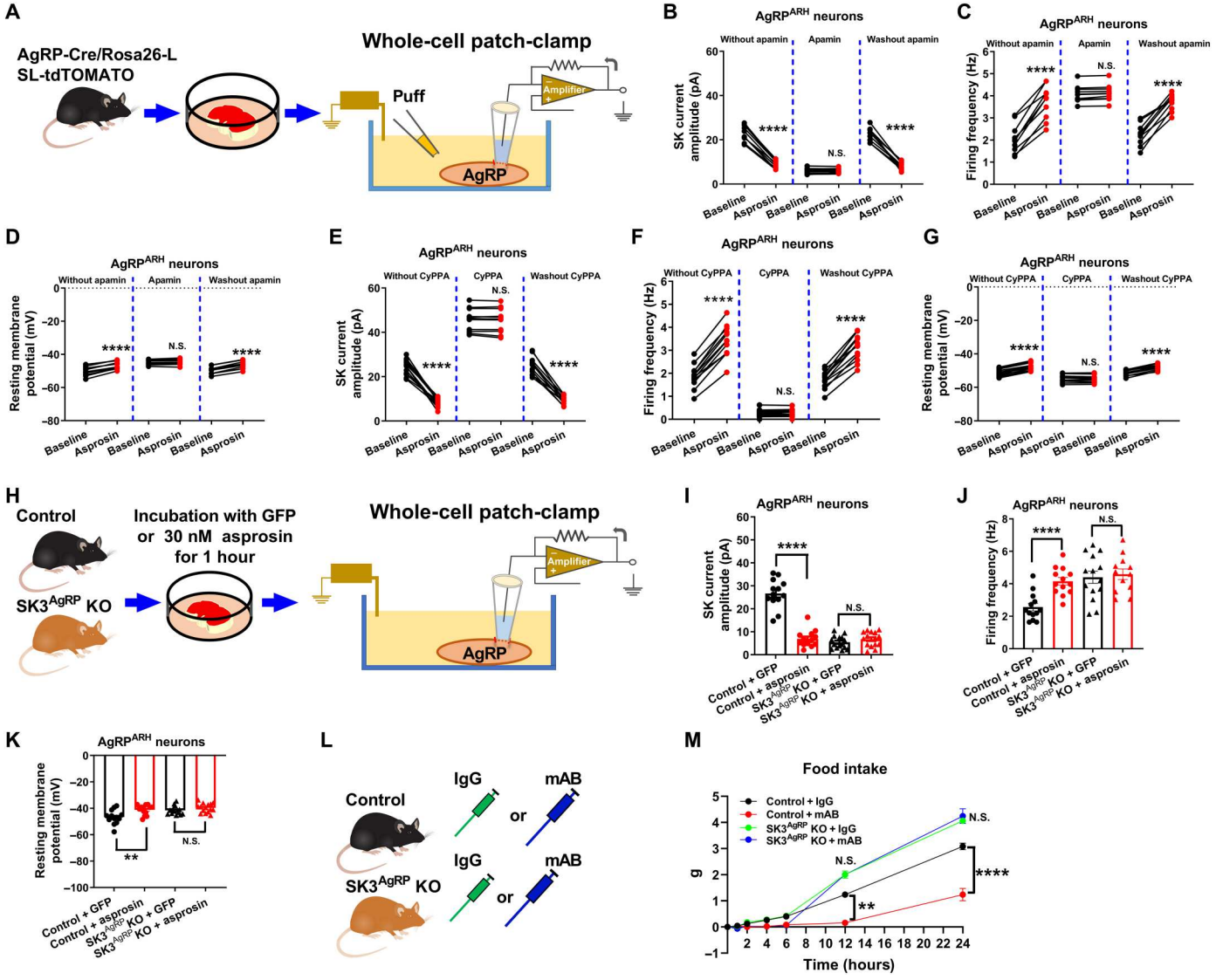

Fig. 4. SK3 is required for the stimulatory effects of asprosin on AgRP^{ARH} neurons and food intake. (**A**) Schematic of AgRP^{ARH} neurons treated with or without apamine or CyPPA for electrophysiology recordings. (**B**) Data analysis of SK current amplitude, (**C**) AP firing frequency, and (**D**) resting membrane potential in AgRP^{ARH} neurons with or without apamin ($n = 14$ in each group). (**E**) Data analysis of SK current amplitude, (**F**) AP firing frequency, and (**G**) resting membrane potential in AgRP^{ARH} neurons with or without CyPPA ($n = 14$ in each group). (**H**) Schematic of control or SK3^{AgRP} KO neuron–containing brain slices incubated with GFP or asprosin for electrophysiology recordings. (**I**) Data analysis of SK current amplitude, (**J**) AP firing frequency, and (**K**) resting membrane potential in control or SK3^{AgRP} KO neurons incubated with GFP or asprosin (1-hour incubation). (**L**) Schematic of control or SK3^{AgRP} KO mice that received IgG or mAb (intraperitoneal injection) under fed condition. (**M**) Food intake at 1, 2, 4, 6, 12, and 24 hours after injection of IgG or mAb. Data are presented as means ± SEM with individual datapoints. $^{**}P < 0.01$ and $^{****}P < 0.0001$ by paired two-sample *t* test (B to G) or unpaired two-sample *t* test (I to K and M).

inhibitor) (*2*, *37*). We found that asprosin failed to reduce the SK current and the firing activity in AgRP^{ARH} neurons in the presence of PKI (fig. S6, C to E). Together, we conclude that asprosin activates AgRP^{ARH} neurons by inhibiting SK current via the Ptprd/PKA signal pathway.

Genetic KO of SK3 from AgRP^{ARH} neurons abolished asprosin's effect in vivo

Last, we used fiber photometry to in vivo test whether asprosin activates AgRP^{ARH} neurons via SK3. Specifically, *AgRP-Cre* (control) and *Kcnn3$^{f/f}$/AgRP-Cre* (SK3^{AgRP} KO) mice were stereotaxically injected with AAV-FLEX-GCaMP6f virus into the ARH (one side). This will allow GCaMP6f to be selectively expressed in the AgRP^{ARH} neurons in control and SK3^{AgRP} KO mice. At the same surgery, we implanted an optical fiber to target ARH and an intracerebroventricular cannula to target the left ventricular (Fig. 7, A and B, and fig. S7, A, B, D, and E). Four weeks after the surgery, we intracerebroventricularly injected GFP (control) or 10 ng of asprosin and continuously recorded the GCaMP fluorescence from 5 min before to 20 min after infusion. During recording, food was removed, and mice were under fed conditions. In the control mice, GFP did not change, but 10 ng of asprosin significantly

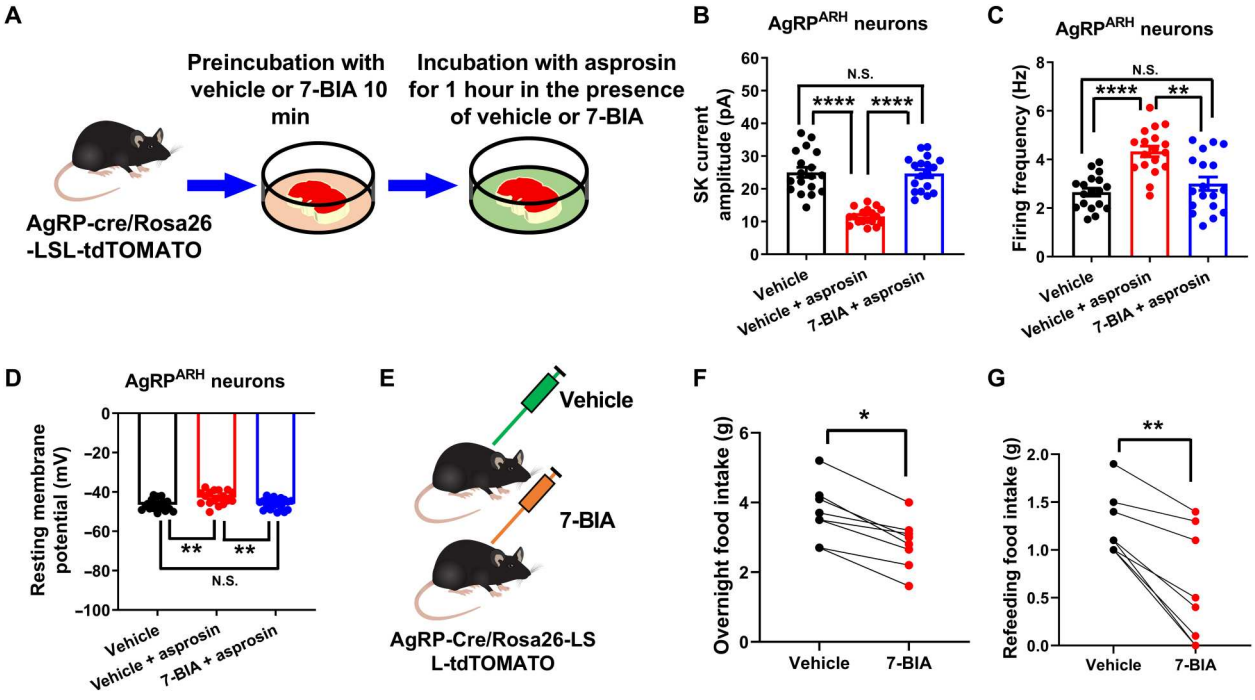

Fig. 5. Pharmacologically blocking Ptprd abolishes asprosin's effect on AgRP^{ARH} neurons and reduces food intake in mice. (**A**) Schematic of asprosin incubation in brain slices containing AgRP^{ARH} neurons pretreated with vehicle or 7-BIA from the *AgRP-Cre/Rosa26-LSL-tdTOMATO* mice. (**B**) Data analysis of SK current amplitude, (**C**) AP firing frequency, and (**D**) resting membrane potential in vehicle, vehicle mixed with asprosin, and 7-BIA mixed with asprosin groups ($n = 18$ from three different animals in each group). (**E**) Schematic of vehicle or 7-BIA intraperitoneal injection in the C57BL/6J mice. (**F**) Overnight food intake after vehicle or 7-BIA injection in mice ($n = 8$). (**G**) Six-hour refeeding food intake after 18 hours of overnight fasting from vehicle- or 7-BIA–injected mice ($n = 8$). Data are presented as means ± SEM with individual datapoints. *$P < 0.05$, **$P < 0.01$, and ****$P < 0.0001$ by unpaired two-sample *t* test (B to D) or paired two-sample *t* test (F and G).

increased the GCaMP signals in AgRP^{ARH} neurons (Fig. 7, C and D), providing in vivo evidence to support the stimulatory effects of asprosin on AgRP^{ARH} neurons. We also observed that a single bolus intracerebroventricular infusion of asprosin significantly increased 24-hour food intake in control mice (Fig. 7E), validating the orexigenic effects. When SK3 was selectively knocked out from AgRP neurons, asprosin failed to increase the GCaMP signals or food intake (Fig. 7, F to H). Notably, we did not observe any changes in signals from the isosbestic channel after asprosin infusion (fig. S7, C and F), excluding potential effects induced by artificial interference. All these data reveal that asprosin activates AgRP^{ARH} neurons to promote food intake through the SK3 ion channel.

DISCUSSION

In this study, we have identified that asprosin used SK3-mediated potassium conductance to activate AgRP^{ARH} neurons and stimulate appetite. The identity of the asprosin orexigenic receptor, Ptprd, was recently reported (*32*). Our current data have confirmed the necessity of Ptprd for asprosin-mediated AgRP^{ARH} neuron activation. Asprosin reduces the SK current in AgRP^{ARH} neurons under fasted conditions via Ptprd. Pharmacologic and genetic blockade of Ptprd in AgRP^{ARH} neurons abolishes asprosin-mediated modulation of the SK current and AgRP^{ARH} neuronal activity under fed conditions (Figs. 5, B to D, and 6, D to F, and fig. S5, C to E). This is consistent with the fact that deletion of *Ptprd* renders mice unresponsive to the orexigenic effects of exogenous asprosin and AgRP^{ARH} neurons unresponsive to the activating effects of asprosin (*7*). Whether the asprosin-Ptprd signaling axis in other brain regions also depends on the modulation of the SK current is still an open question that warrants further studies. In AgRP^{ARH} neurons, however, the answer is unequivocal: Modulation of the SK current, particularly through the SK3 channel, is necessary for asprosin-mediated AgRP^{ARH} neuron activation and appetite stimulation.

We previously reported that the dynamic expression of SK3 channels in AgRP^{ARH} neurons mediates the dynamic firing activities of these neurons during the fed-to-fasted transition (*17*). Asprosin was also reported to be significantly increased in the circulation and CSF after fasting as asprosin could cross the blood-brain barrier (*2*), suggesting a potential link between asprosin and SK channels. In the current study, we confirmed that asprosin induced SK3 level changes during fasting. SK current was significantly increased in asprosin-deficient mice and mice with AgRP^{ARH} neuron–specific *Ptprd* KO or KD. All these data indicate that the hunger hormone asprosin regulates SK3 via Ptprd signaling.

However, it is still uncertain to which extent the AgRP^{ARH} neurons depend on SK3 to respond to asprosin. On the basis of several key findings, we speculate that a large portion of AgRP^{ARH} neurons shows SK3 dependence on asprosin's effects. First, most AgRP^{ARH} neurons express SK3 (91%) based on our immunostaining data from well-fed male WT mice (fig. S3). Second, our ex vivo recording demonstrated that 64% of AgRP^{ARH} neurons are directly activated by asprosin in the presence of synaptic blockers (fig. S1E), consistent with the coexpression levels (68%) of Ptprd in AgRP^{ARH} neurons. All these asprosin-responsive AgRP neurons have SK3

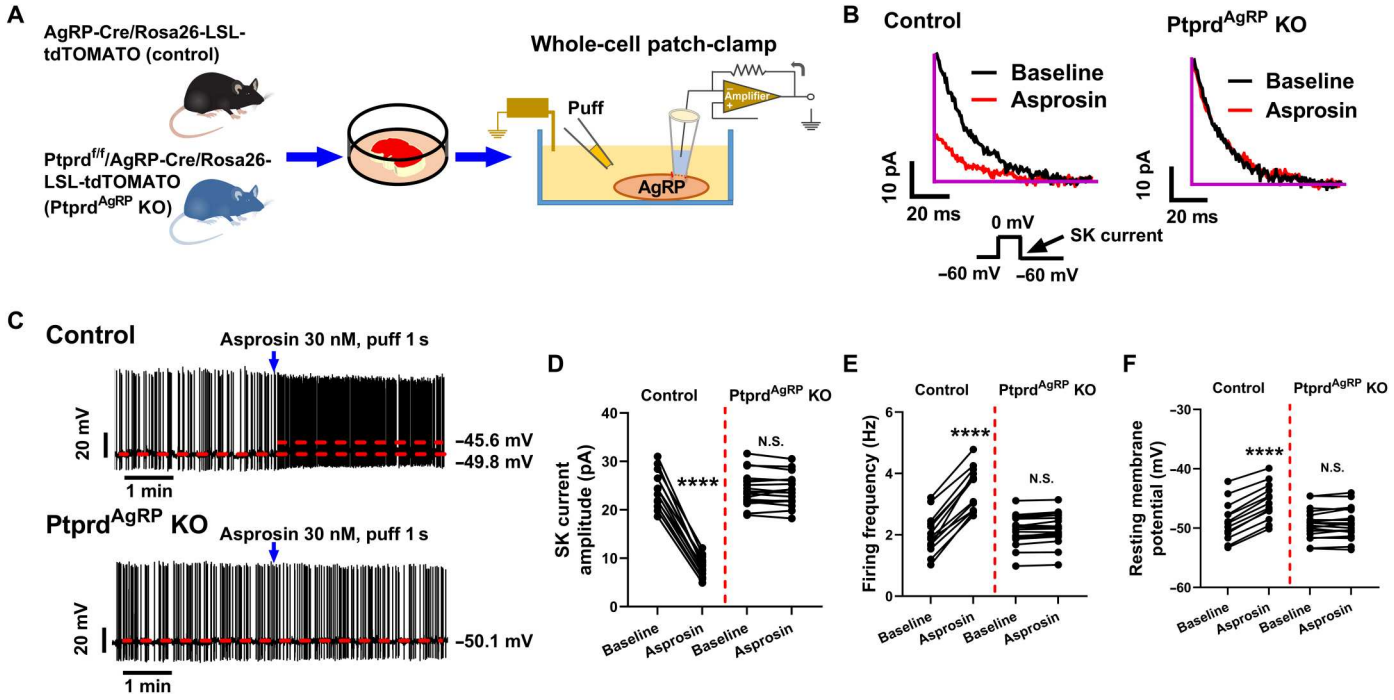

Fig. 6. Selective deletion of Ptprd from AgRP^{ARH} neurons abolishes asprosin-induced SK current inhibition and neural activation. (**A**) Schematic of *AgRP-Cre/Rosa26-LSL-tdTOMATO* (control) or *Ptprd$^{f/f}$/AgRP-Cre/Rosa26-LSL-tdTOMATO* mice (Ptprd^{AgRP} KO) for electrophysiology recordings. (**B**) Representative SK current traces from control and Ptprd^{AgRP} KO neurons. (**C**) Representative AP firing traces from control and Ptprd^{AgRP} KO neurons. (**D**) Data analysis of SK current amplitude, (**E**) AP firing frequency, and (**F**) resting membrane potential in control or Ptprd^{AgRP} KO neurons after asprosin puff treatment (1 s, 30 nM; $n = 13$ or 19 from three different animals in each group). Data are presented as means ± SEM with individual datapoints. ****$P < 0.0001$ by paired two-sample t test (D to F).

current. Last, genetic deletion of SK3 or Ptprd in AgRP^{ARH} neurons abolished the stimulatory effects of asprosin on all ex vivo recorded AgRP^{ARH} neurons (Figs. 4, I to K, and 6, D to F) and in vivo recorded GCaMP signal from AgRP^{ARH} neurons (Fig. 7, F to H). One caveat of the in vivo fiber photometry study is that artificial intracerebroventricular infusion of asprosin may not fully recapitulate the normal physiologic concentration and endogenous actions of asprosin, which could be further addressed in future studies. On the basis of all these data, we conclude that asprosin′s effect on AgRP neurons highly depends on both Ptprd and SK3. Certainly, SK3 may not be the only mediator for the dynamic changes in AgRP^{ARH} neuronal firing activities. It is reported that a delayed rectifier Kv channel (Kv7.3) can be modified by O-GlcNAc transferase after food deprivation (*38*). Thus, we could not exclude the possibility that asprosin may also regulate other ion channels via the Ptprd in AgRP^{ARH} neurons.

It was reported that Ptprd is highly expressed in AgRP^{ARH} neurons (*16*), and Ptprd is the asprosin receptor in AgRP neurons (*7*). It was also reported that increased plasma asprosin through an adenoviral-mediated approach failed to increase appetite in *Ptprd$^{-/-}$* mice compared with WT (*7*). Our current data further confirmed that asprosin directly targets Ptprd in hypothalamic AgRP^{ARH} neurons to activate AgRP^{ARH} neurons and feeding. We showed that pharmacological and genetic blockage of Ptprd in AgRP^{ARH} neurons abolished the activation of asprosin′s effect on the excitation of AgRP^{ARH} neurons. Asprosin could no longer inhibit SK current in AgRP^{ARH} neurons with the loss of Ptprd function. These results further support that Ptprd is upstream of SK current, and asprosin activates AgRP^{ARH} neurons and feeding through Ptprd-mediated inhibition of SK current. However, the pathway from Ptprd to SK current warrants further studies. We previously showed that asprosin/Ptprd signaling modulates the firing activity of AgRP neurons via the PKA pathway (*2*). The SK channel has been reported to be inhibited by the cAMP-dependent PKA pathway, which plays an integral role in SK channel gating (*39*–*43*), suggesting a potential link between Ptprd and SK3 via PKA. Consistently, we found that asprosin-induced inhibition of SK current and stimulation of membrane potential and firing frequency in AgRP^{ARH} neurons were abolished by cotreatment of PKI, a selective PKA antagonist. These findings support a mediating role of the PKA pathway in Ptprd′s inhibitory effects on the SK3 channel.

Mechanistically, cAMP-dependent PKA signaling has been shown to reduce SK current by suppressing cell surface expression and nanoclusters of SK channels in neurons (*44*). PKA directly phosphorylates SK channels at multiple sites to remove them from the cell surface and restrict them in the endoplasmic reticulum (*41*). With tonic cAMP-PKA levels, SK channels are primarily located in dendrites with a limited expression on somatic membranes (*45*, *46*). Most somatic SK channels (SK1, SK2, and SK3) are internalized and retained on the rough endoplasmic reticulum (*45*, *47*, *48*). The pharmacological blockade of PKA signaling increases the somatic surface expression of SK channels by redistributing intracellular SK channels to the membrane (*44*), suggesting a regulatory role of PKA on the membrane location of SK channels. The asprosin/Ptprd axis likely activates the cAMP-PKA pathway to

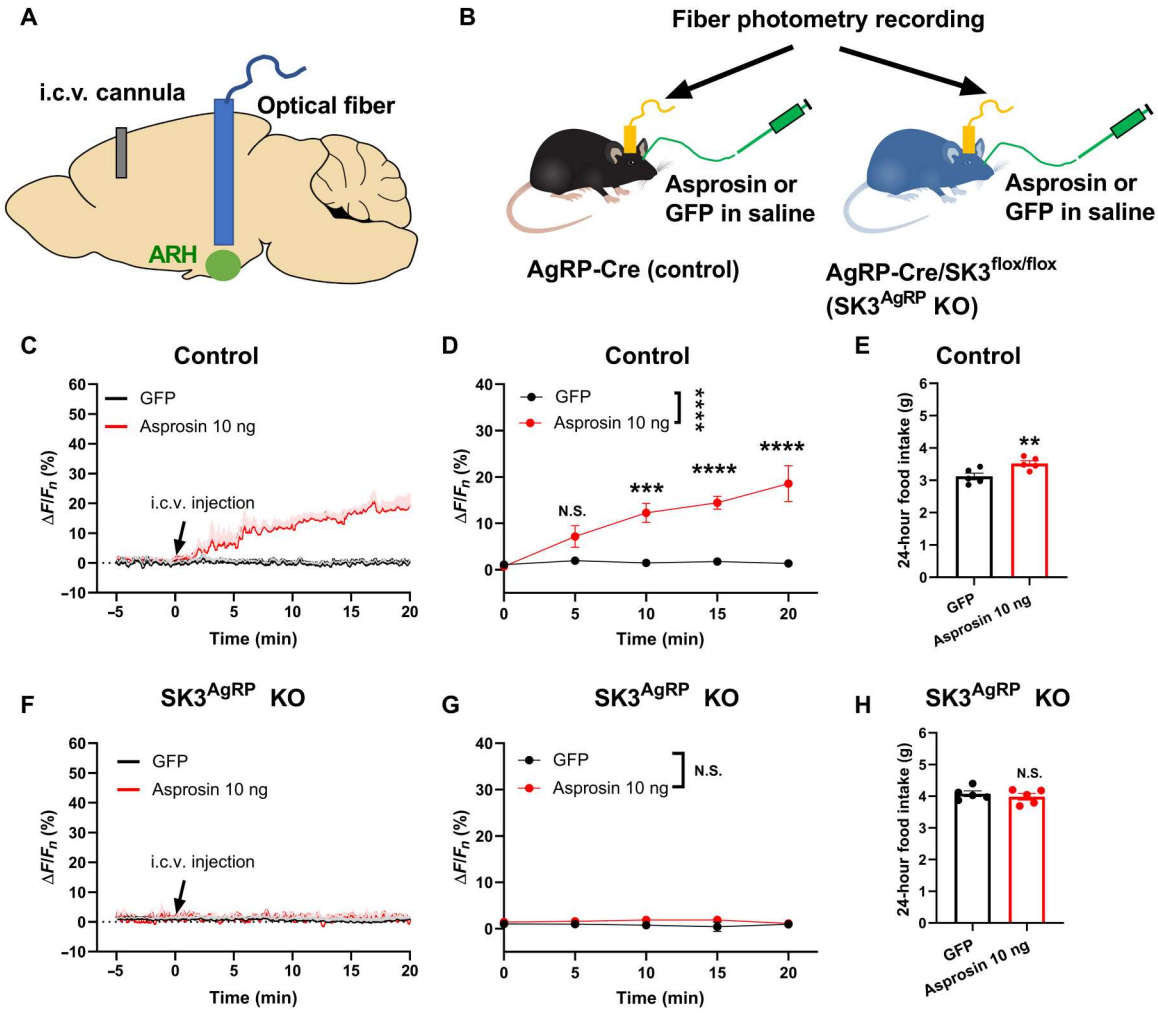

Fig. 7. Selective deletion of SK3 from AgRP^{ARH} neurons abolished asprosin's effect in vivo. (**A** and **B**) Schematic of intracerebroventricular (i.c.v.) cannulation and optical fiber implantation in *AgRP-Cre* (control) or *Kcnn3$^{f/f}$/AgRP-Cre* (SK3^{AgRP} KO) for fiber photometry recordings. (**C**) Representative GCaMP6 fluorescence traces from control mice after intracerebroventricular injection of GFP or asprosin. (**D**) Data analysis of GCaMP6 fluorescence from control mice after intracerebroventricular injection of GFP or asprosin at 0, 5, 10, 15, and 20 min ($n = 5$ in each group). (**E**) Twenty-four-hour food intake in the control mice after intracerebroventricular injection of GFP or asprosin ($n = 5$ in each group). (**F**) Representative GCaMP6 fluorescence traces from SK3^{AgRP} KO mice after intracerebroventricular injection of GFP or asprosin. (**G**) Data analysis of GCaMP6 fluorescence from SK3^{AgRP} KO mice at 0, 5, 10, 15, and 20 min after intracerebroventricular injection of GFP or asprosin ($n = 5$ in each group). (**H**) Twenty-four-hour food intake in the SK3^{AgRP} KO mice after intracerebroventricular injection of GFP or asprosin ($n = 5$ in each group). Data are presented as means ± SEM with individual data points. **P < 0.01, ***P < 0.001, and ****P < 0.0001 by two-way ANOVA analysis followed by post hoc Sidak tests (D and E).

internalize the SK3 channel and to limit the membrane availability of SK3 channel. Notably, inhibition of PKA has also been reported to promote the transition from single entities to a group of multiple SK channels in nanodomains on the cell surface, suggesting enhanced conductance (*44*). Hence, it is also possible that the asprosin/Ptprd axis activates PKA to increase the percentage of the single SK channel in nanodomains, resulting in reduced conductance. These potential rapid mechanisms are consistent with our observations that the puff treatment of asprosin inhibits SK current within minutes (figs. S1A and S6C). However, further studies are warranted to clarify the specific mechanism by which asprosin/Ptprd/PKA axis modulates SK current.

Another interesting finding is that chronically increased circulating asprosin by AAV vector infection significantly reduced the protein expression of SK3 in the AgRP^{ARH} neurons, suggesting inhibitory effects of asprosin on SK3 expression. Although the asprosin/Ptprd/PKA axis likely contributes to enhanced SK channel activity via posttranslational modifications (phosphorylation), as far as we know, there are limited reports on the regulatory effects of PKA on SK channel expression. Several studies instead demonstrate the dissociation of functional up-regulation of membrane SK channel and increased expression levels of SK channel (*43*, *49*, *50*). The asprosin-induced inhibition of SK3 expression (chronic response) may be mediated through an intracellular mechanism independent of PKA signaling (acute response). Future research efforts will be needed to further investigate the potential mechanisms mediating the role of asprosin in SK3 channel expression.

Notably, the activities of AgRP^{ARH} neurons are tightly regulated by nutritional status. For example, AgRP^{ARH} neurons in satiated animals are inhibited and are less sensitive to food cues (*51*, *52*).

On the other hand, fasting enhances AgRP^{ARH} neuronal activity (*2*, *17*, *52*), which promotes food intake. Asprosin is reported to be elevated in fasted animals (*1*, *2*). AgRP^{ARH} neuronal activity and associated appetite stimulation during fasting appear to depend on asprosin-Ptprd signaling (*7*). Another well-known hormone that up-regulates AgRP^{ARH} neuronal activity and stimulates appetite, ghrelin, has no impact whatsoever on SK current in AgRP^{ARH} neurons nor does it require SK3 to activate AgRP^{ARH} neurons. This suggests that the use of the SK current and the SK3 channel is unique to asprosin′s mechanism of action, providing a clear departure from that of ghrelin′s.

Besides AgRP neurons, many other hypothalamic neurons also play important roles in feeding and glucose balance. We have previously reported that asprosin failed to directly regulate some neuron types including POMC-expressing neurons, serotonin neurons, dopamine neurons, steroidogenic factor-1 neurons, and neuron populations in the paraventricular hypothalamic nucleus neurons (*2*), which are relevant for feeding and glucose homeostasis. However, some other neuron types—including the cannabinoid receptor 1–expressing neurons (*53*), pituitary adenylate cyclase–activating polypeptide–releasing neurons (*54*), neuronal nitric oxide synthase–expressing neurons (*55*, *56*), and brain-derived neurotrophic factor–releasing neurons (*57*)—in the ventral medial of hypothalamus (VMH) have been identified for the regulation of food intake, glucose homeostasis, and energy expenditure. It is possible that apsrosin also acts on those VMH neuron populations to further regulate feeding behavior and glucose homeostasis. Recent studies revealed that γ-aminobutyric acid (GABA)–releasing neurons in the lateral hypothalamus are associated with feeding behavior (*58*). Optogenetic stimulation of mouse zona incerta (ZI) GABA neurons immediately evoked binge-like eating within 2 to 3 s (*59*). When ZI GABA neurons were ablated, animals displayed reduced body weight (*59*). Thus, it will be interesting to further validate whether asprosin could act on those hypothalamic GABA neurons to regulate feeding behavior and body weight gain.

In summary, our results support a model where the hunger hormone asprosin regulates SK3 in AgRP^{ARH} neurons to promote feeding via the Ptprd/PKA signal pathway. On one hand, when animals are satiated, a low level of asprosin in the plasma maintains SK3 at a high level in AgRP^{ARH} neurons, leading to their inhibition and likely preventing animals from overeating. On the other hand, when animals are fasted, increased asprosin in the plasma reduces SK3-mediated current in AgRP^{ARH} neurons to stimulate AgRP^{ARH} neuronal firing activity and stimulate appetite (Fig. 8). Selective deletion of Ptprd or SK3 in AgRP^{ARH} neurons abolishes these asprosin-mediated effects. Identification of the underlying current and specific ion channel for asprosin-Ptprd mediated AgRP^{ARH} neuronal activity and orexigenic effects is a major step forward in our understanding of mammalian energy balance regulation. It also provides an additional target for pharmacologic manipulation for the treatment of obesity and metabolic syndrome.

MATERIALS AND METHODS

Mice

WT C57BL/6 mice (WT mice; JAX #000664), *Rosa26-LSL-tdTOMATO* or Ai14 mice (Jackson Laboratory, JAX #007914), *AgRP*-Cre [C57BL/6-Agrptm1(cre) Lowl or *Agrp-IRES-Cre*; Jackson Laboratory, JAX #012899], *Fbn1*$^{NPS/+}$ (*2*) (C57BL/6-Fbn1em1Chop/J; Jackson Laboratory, JAX #033548), and *Kcnn3*$^{f/f}$ mice (*60*) (Jackson Laboratory, JAX #019083) were purchased from The Jackson Laboratory. We crossed the *Kcnn3*$^{f/f}$ mice with recently tamoxifen-inducible *AgRP-CreERT2* mice (*35*) to generate *Kcnn3*$^{f/f}$/*AgRP-CreERT2* (SK3^{AgRP} KO) and their control littermates (*Kcnn3*$^{f/+}$/*AgRP-CreERT2* and *Kcnn3*$^{+/+}$/*AgRP-CreERT2*). Homozygous, conditionally ready floxed mice *Ptprd*$^{f/f}$ [Ptprd tm2c(KOMP)Wtsi] (*7*) were mated with *AgRP-Cre* to create AgRP neuron–specific KO of Ptprd (Ptprd^{AgRP} KO). *Kcnn3*$^{f/f}$ mice were crossed with *AgRP-Cre* to generate the *Kcnn3*$^{f/f}$/*AgRP-Cre* (SK3^{AgRP} KO) mice for the fiber photometry experiment. In some breedings, we also introduced the *Rosa26-tdTOMATO* allele onto *AgRP-Cre*, *Ptprd*$^{f/f}$/*AgRP-Cre*, *AgRP-CreERT2*, and *Kcnn3*$^{f/f}$/*AgRP*-CreERT2 mice, respectively. These crosses generated control, Ptprd^{AgRP} KO, and SK3^{AgRP} KO mice with TOMATO selectively expressed in AgRP^{ARH} neurons (after tamoxifen inductions). These mice were used for electrophysiological studies. For conditional KO of *Ptprd* in adult mice, CRISPR-cas9–mediated unilateral and bilateral KO was done in *AgRP*-Cre mice.

Mice were housed in microventilators on a 12-hour light cycle and were fed normal chow (5V5R or 5015, Lab Supply). Animal housing, husbandry, and euthanasia were conducted under animal protocols approved by the Institutional Animal Care and Use Committee of Baylor College of Medicine, Pennington Biomedical Research Center, and Case Western Reserve University.

KD of *Ptprd* in AgRP^{ARH} neurons in adult mice

CRISPR-Cas9 approach was used for unilateral and bilateral disruption of *Ptprd* selectively in AgRP^{+} neurons as we reported previously (*7*). Briefly, targeting efficiency of sgRNA *GTCAGCAACCAGA GATTTGA* against *Ptprd* was tested and confirmed with TIDE analysis (*61*) before being cloned into AAV-ITR-U6-sgRNA plasmid. To knock down *Ptprd* only in AgRP^{ARH} neurons, *AgRP-Cre* male mice (10 to 12 weeks of age) received stereotaxic injections of AAV-FLEX-saCas9 (Vector Biolabs, #7122) with AAV-Ptprd/sgRNA-FLEX-GFP on one side and AAV-Ptprd/sgRNA-FLEX-GFP with AAV-mCherry (no Cas9) virus on the other side in the ARH. Six weeks after the stereotaxic injections, electrophysiology recordings in GFP-labeled AgRP^{+} neurons from each side of ARH (control versus Ptprd-KD side) were performed.

Electrophysiology

AgRP^{ARH} neuron labeling and electrophysiology experiments were performed as previously described (*2*, *7*, *17*). Briefly, to identify AgRP^{ARH} neurons, we crossed the *Rosa26-LSL-tdTOMATO* (JAX #007914) mice with *AgRP-Cre* mice (JAX #012899) to generate *AgRP*-Cre/Rosa26-LSL-tdTOMATO mice, which express TOMATO selectively in AgRP^{ARH} neurons. In some experiments, we also crossed *Fbn1*$^{NPS/+}$ mice (JAX #033548) with *Agrp-Cre*/*Rosa26-LSL-tdTOMATO* mice to generate *Fbn1*$^{NPS/+}$/*AgRP-Cre*/*Rosa26-LSL-tdTOMATO* mice. In some experiments, we introduced *Rosa26-LSL-tdTOMATO* allele onto *Ptprd*$^{f/f}$/*AgRP-Cre*, *AgRP-CreERT2*, and *Kcnn3*$^{f/f}$/*AgRP-CreERT2* mice, respectively.

Following procedures previously described by Mishra *et al.* (*7*), on the day of electrophysiology recording experiment, mice were euthanized under fed or fasted conditions. Then, the entire brains of the mice were removed and immediately submerged in ice-cold sucrose-based cutting solution (adjusted to pH 7.3) containing 10 mM NaCl, 25 mM $NaHCO_3$, 195 mM sucrose, 5 mM glucose, 2.5

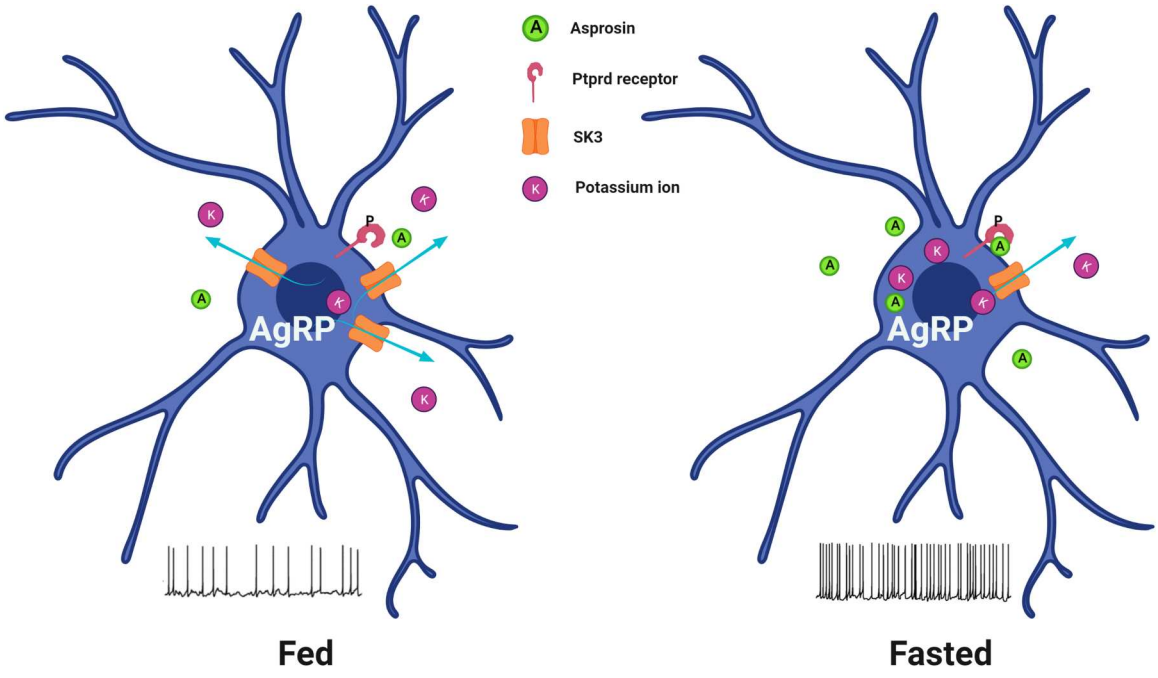

Fig. 8. Hunger hormone asprosin activates AgRP^{ARH} neurons via an SK-dependent mechanism.

mM KCl, 1.25 mM NaH_2PO_4, 2 mM Na pyruvate, 0.5 mM $CaCl_2$, and 7 mM $MgCl_2$ bubbled continuously with 95% O_2 and 5% CO_2 (*2*, *17*, *18*). The slices (250 μm) were cut with a Microm HM 650 V vibratome (Thermo Fisher Scientific) or VT1200 S vibratome (Leica) and recovered for 1 hour at 34°C and then maintained at room temperature in artificial CSF (aCSF; pH 7.3) containing 126 mM NaCl, 2.5 mM KCl, 2.4 mM $CaCl_2$, 1.2 mM NaH_2PO_4, 1.2 mM $MgCl_2$, 11.1 mM glucose, and 21.4 mM $NaHCO_3$ saturated with 95% O_2 and 5% CO_2. TOMATO(+) neurons were visualized using epifluorescence and infrared–differential interference contrast (IR-DIC) imaging on an upright microscope equipped with a moveable stage (MP-285, Sutter Instrument).

For electrophysiological recording, brain slices were superfused at 34°C in oxygenated aCSF at a flow rate of 1.8 to 2 ml/min as described previously (*7*). Patch pipettes with resistances of 3 to 5 megohms were filled with intracellular solution (pH 7.3) containing 128 mM K-gluconate, 10 mM KCl, 10 mM Hepes, 0.1 mM EGTA, 2 mM $MgCl_2$, 0.05 mM Na-GTP, and 0.05 mM Mg-ATP. Recordings were made using a MultiClamp 700B amplifier (Axon Instrument), sampled using Digidata 1440A, and analyzed offline with pClamp 10.3 software (Axon Instruments). Series resistance was monitored during the recording, and the values were generally <10 megohms and were not compensated. Data were excluded if the series resistance increased markedly during the experiment or without overshoot for the AP. Currents were amplified, filtered at 1 kHz, and digitized at 20 kHz (*7*). The current clamp was engaged to test neural firing frequency and resting membrane potential in control and Ptprd^{AgRP} KO neurons after GFP or asprosin treatment (1-s puff, 30 nM).

The method of KD of *Ptprd* using CRISPR-cas9 in mice was published previously (*7*). Briefly, *AgRP-Cre* mice 10 to 12 weeks of age received stereotaxic injections of AAV-FLEX-saCas9 + AAV-*Ptprd*/sgRNA-FLEX-GFP or AAV-*Ptprd*/sgRNA-FLEX-GFP + AAV-mCherry (no Cas9) in ARH [anteroposterior, −1.70 mm; mediolateral, ±0.25 mm; and dorsoventral, −5.90 mm]. The electrophysiology recording of GFP-labeled or mCherry-labeled AgRP$^+$ neurons was performed 4 weeks after surgery. Mice were maintained under ad libitum feeding. On the day of recording, fed mice were deeply anesthetized with isoflurane and were transcardially perfused, and brain slices containing the ARH were prepared and maintained in aCSF as described above. GFP- or mCherry-labeled neurons in the ARH were visualized using epifluorescence and IR-DIC imaging on an upright microscope (Eclipse FN-1, Nikon).

In another experiment, brain slices containing the ARH were prepared from *AgRP-Cre/Rosa26-LSL-tdTOMATO* mice (10 to 12 weeks of age) using same method described above. TOMATO(+) AgRP^{ARH} neuron depolarization and firing rate were recorded in response to asprosin alone (1-hour incubation) and asprosin preincubated with 7-BIA (10 μM, 10 min) or vehicle or a physiologically irrelevant protein (GFP, 1-hour incubation). In some experiments, apamin-sensitive outward tail currents (SK currents) were recorded as described previously with some modifications (*62*, *63*). SK currents in AgRP neurons were recorded under a voltage clamp in the presence of TTX with a 400-ms depolarizing pulse (from −60 to 0 mV and back to −60 mV, holding at −60 mV) (*17*, *63*, *64*).

Chronic overexpression of asprosin

C57BL/6J or *AgRP-Cre/Rosa26-LSL-tdTOMATO* littermate male mice (12 to 14 weeks old) were injected intravenously via the tail vein with AAV8 as previously described (*7*, *32*). Mice injected with AAV8-empty (1×10^{12} genome copy (GC) per mouse) served as controls for experimental mice that received AAV8-IL2sp-6His-Asprosin (1×10^{12} GC per mouse) containing an N-terminal his-tagged human asprosin coding region preceded by an IL-2 signal peptide, under the control of an EF1 promoter.

Glucose tolerance test

For glucose tolerance test (GTT), overnight fasting mice were intraperitoneally injected with glucose solution (2 g/kg of body mass), and blood glucose levels were measured at 0, 15, 30, 60, and 120 min after treatment. Mouse glucose was determined using a handheld glucometer (OneTouch Ultra2, LifeScan) from a droplet of tail blood.

Food intake and body weight assessment

In some experiments, control or AAV-asprosin overexpression mice were singly housed. Average food intake and body weight were measured weekly. In some experiments, food intake was measured in mice that received intraperitoneal injection of 50 μg of 7-BIA dissolved in dimethyl sulfoxide (DMSO)–saline or the vehicle DMSO-saline. For 7-BIA experiments, mice were acclimated to single housing in standard caging and fed a pelleted, dustless diet (F0173, Bio-Serv) for 3 days before manual measurement of food intake. For overnight food intake measurement, mice were injected with 7-BIA or the vehicle 10 min before lights off, and cumulative food intake was measured for the duration of 6:00 p.m. to 10:00 a.m. For measuring 6-hour refeeding cumulative food intake, mice were fasted for 18 hours (4:00 p.m. to 10:00 a.m.), followed by free access to measured amount of food and 7-BIA or vehicle treatment at 10:00 a.m. Six-hour refeeding cumulative food intake was measured at 4:00 p.m. In mAb food intake experiment, control or $SK3^{AgRP}$ KO mice were fed on high-fat diet. Mice received anti-asprosin mAb or IgG intraperitoneal injection before the light turned off. Food intake was measured using the BioDAQ system.

Asprosin ELISA detection procedures

The detection of asprosin was described previously (*2*, *32*). Briefly, a sandwich enzyme-linked immunosorbent assay (ELISA) custom built using mouse monoclonal anti-asprosin antibody against human asprosin amino acids 106 to 134 (human profibrillin amino acids 2838 to 2865) as the capture antibody and a rabbit anti-asprosin mAb as the detection antibody were used for the detection of human asprosin (*2*, *32*). An anti-rabbit secondary antibody linked to horseradish peroxidase was used to generate a signal, and mammalian cell–produced recombinant human asprosin was used to generate a standard curve.

Validation of *Kcnn3* and *Ptprd* deletion in AgRP neurons

At 9:00 a.m., fed male *Kcnn3*$^{f/f}$*/AgRP-CreERT2/Rosa26-LSL-tdTOMATO*, *AgRP-CreERT2/Rosa26-LSL-tdTOMATO*, *Ptprd*$^{f/f}$*/AgRP-Cre/Rosa26-LSL-tdTOMATO*, and *AgRP-Cre/Rosa26-LSL-tdTOMATO* mice were anesthetized with inhaled isoflurane and perfused with saline, followed by 10% formalin. Brain sections (25 μm in thickness) were collected and then subjected to dual immunofluorescence for SK3 and Ptprd. Briefly, one series of the brain sections were blocked (5% normal donkey) for 1 hour. Then, the brain sections were incubated overnight with rabbit anti-SK3 antibody (1:500 dilution; #APC-025, Alomone Labs) or rabbit anti-Ptprd antibody (1:1000 dilution; #A15713, ABclonal) on a shaker at 4°C overnight. The next day, the brain sections were incubated with the donkey anti-rabbit Alexa Fluor 488 (1:500; A21206, Invitrogen) for 2 hours. Sections were mounted on slides and coverslipped with 4′,6-diamidino-2-phenylindole mounting medium. Fluorescence images were taken using the Leica 5500 fluorescence microscope with OptiGrid structured illumination. AgRP neurons coexpressed by SK3 or Ptprd were counted and averaged in at least four consecutive coronal brain sections containing the ARH from each mouse, and these data were treated from one biological sample. Data from four different mice were used in statistical analyses.

Fiber photometry

To record the activity of AgRP neurons in freely moving mice, male *AgRP-Cre* or *Kcnn3*$^{f/f}$*/AgRP-Cre* mice (10 weeks of age) were anesthetized by isoflurane and received stereotaxic injections of 200 nl of AAV-FLEX-GCaMP6f virus (#AV7609, UNC Vector Core; 3.7×10^{12} viral genomes/ml) into the ARH (AP, −1.70 mm; ML, +0.25 mm; and DV, −5.90 mm) using a stereotaxic instrument with nonpuncture ear bars (RWD Life Science). During the same surgery, an optical fiber (fiber: core = 400 μm; 0.39 numerical aperture; M3 thread titanium receptacle; RWD Life Science) was implanted over the ARH (anteroposterior, −1.70 mm; mediolateral, +0.25 mm; and dorsoventral, −5.70 mm). During the same surgery, stainless steel intracerebroventricular cannulas (RWD Life Science) were inserted into the lateral ventricles (intracerebroventricular coordinates without angle: anteroposterior, 0.34 mm; mediolateral, −1.00 mm; and dorsoventral, 2.30 mm) with 5° angle rotated clockwise (modified coordinates with 5° angle: anteroposterior, 0.34 mm; mediolateral, −1.20 mm; and dorsoventral, 2.31 mm). Optical fibers and cannulas were fixed to the skull by using dental acrylic. Mice were individually housed for at least 3 weeks after surgery before acclimating to the investigator′s handling for 1 week before the recordings.

Mice were allowed to adapt to the tethered patchcord for 2 days before experiments and given 5 min to acclimate to the tethered patchcord before any recording. Fiber photometry recordings of AgRP neurons were done in mice at fed condition without food. All the control or $SK3^{AgRP}$ KO mice received intracerebroventricular injection of GFP (as control) and 10 ng of asprosin (in 1 μl of saline) on different days. There was a 1-week washout period between each injection. Each mouse was recorded for a 5-min baseline and 20 min after intracerebroventricular injections. All the mice were returned to their home cages, and food intake was monitored for 24 hours after intracerebroventricular injections.

The fiber photometry recording was carried out using a commercial device (RWD Life Science) as previously described (*65*–*67*). For each recording, continuous 30-μW blue light-emitting diode (LED) at 470 nm and 15-μW ultraviolet (UV) LED at 410 nm served as excitation light sources, driven by an R810 dual-color multichannel fiber photometry system (RWD Life Science). GCaMP6 calcium GFP signals and UV autofluorescent signals were collected through the same fibers back to the R810 system. We derived the values of GCaMP fluorescence change ($\Delta F/F_n$) by calculating $(F_{470} - F_0)/F_0$, where F_0 is the 5-min average baseline fluorescence of the F_{470} channel before the intracerebroventricular injection. The F_{410} channel is used as an isosbestic fluorescence channel; we derived the values of isosbestic fluorescence change ($\Delta F/F_n$) by calculating $(F_{410} - F_0)/F_0$, where F_0 is the 5-min average baseline fluorescence of the F_{410} channel before the intracerebroventricular injection.

Statistical analyses

All results are presented as means ± SEM. Statistical significance was tested using paired two-tailed *t* tests, unpaired two-tailed *t* tests, or analysis of variance (ANOVA; one-way and two-way,

when appropriate), followed by the Sidak multiple comparisons post hoc analysis using GraphPad Prism 8 and 9.

Study approval

Care of all animals and procedures were approved by the Institutional Animal Care and Use Committee of Baylor College of Medicine, Pennington Biomedical Research Center, and Case Western Reserve University.

Supplementary Materials

This PDF file includes:

Figs. S1 to S7

View/request a protocol for this paper from *Bio-protocol*.

REFERENCES AND NOTES

1. C. Romere, C. Duerrschmid, J. Bournat, P. Constable, M. Jain, F. Xia, P. K. Saha, M. Del Solar, B. Zhu, B. York, P. Sarkar, D. A. Rendon, M. W. Gaber, S. A. LeMaire, J. S. Coselli, D. M. Milewicz, V. R. Sutton, N. F. Butte, D. D. Moore, A. R. Chopra, Asprosin, a fasting-induced glucogenic protein hormone. *Cell* **165**, 566–579 (2016).
2. C. Duerrschmid, Y. He, C. Wang, C. Li, J. C. Bournat, C. Romere, P. K. Saha, M. E. Lee, K. J. Phillips, M. Jain, P. Jia, Z. Zhao, M. Farias, Q. Wu, D. M. Milewicz, V. R. Sutton, D. D. Moore, N. F. Butte, M. J. Krashes, Y. Xu, A. R. Chopra, Asprosin is a centrally acting orexigenic hormone. *Nat. Med.* **23**, 1444–1453 (2017).
3. S. Chen, X. Wang, C. M. Qiu, J. N. Hou, X. Y. Wei, C. X. Xiang, M. Y. Tang, R. Zhang, H. F. Pei, Study of the role and mechanism of asprosin/spartin pathway in cardiac microvascular endothelial injury induced by diabete mellitus. *Sichuan Da Xue Xue Bao Yi Xue Ban* **50**, 827–834 (2019).
4. E. Sunnetci Silistre, H. U. Hatipoğlu, Increased serum circulating asprosin levels in children with obesity. *Pediatr. Int.* **62**, 467–476 (2020).
5. M. Yuan, W. Li, Y. Zhu, B. Yu, J. Wu, Asprosin: A novel player in metabolic diseases. *Front. Endocrinol.* **11**, 64 (2020).
6. E. Li, H. Shan, L. Chen, A. Long, Y. Zhang, Y. Liu, L. Jia, F. Wei, J. Han, T. Li, X. Liu, H. Deng, Y. Wang, OLFR734 mediates glucose metabolism as a receptor of asprosin. *Cell Metab.* **30**, 319–328.e8 (2019).
7. I. Mishra, W. R. Xie, J. C. Bournat, Y. He, C. Wang, E. S. Silva, H. Liu, Z. Ku, Y. Chen, B. O. Erokwu, P. Jia, Z. Zhao, Z. An, C. A. Flask, Y. He, Y. Xu, A. R. Chopra, Protein tyrosine phosphatase receptor δ serves as the orexigenic asprosin receptor. *Cell Metab.* **34**, 549–563.e8 (2022).
8. C. T. Bond, J. Maylie, J. P. Adelman, Small-conductance calcium-activated potassium channels. *Ann. N. Y. Acad. Sci.* **868**, 370–378 (1999).
9. W. A. Yuhas, P. A. Fuchs, Apamin-sensitive, small-conductance, calcium-activated potassium channels mediate cholinergic inhibition of chick auditory hair cells. *J. Comp. Physiol. A* **185**, 455–462 (1999).
10. M. Kohler, B. Hirschberg, C. T. Bond, J. M. Kinzie, N. V. Marrion, J. Maylie, J. P. Adelman, Small-conductance, calcium-activated potassium channels from mammalian brain. *Science* **273**, 1709–1714 (1996).
11. J. P. Adelman, J. Maylie, P. Sah, Small-conductance Ca^{2+}-activated K^+ channels: Form and function. *Annu. Rev. Physiol.* **74**, 245–269 (2012).
12. D. Dulon, L. Luo, C. Zhang, A. F. Ryan, Expression of small-conductance calcium-activated potassium channels (SK) in outer hair cells of the rat cochlea. *Eur. J. Neurosci.* **10**, 907–915 (1998).
13. X. M. Xia, B. Fakler, A. Rivard, G. Wayman, T. Johnson-Pais, J. E. Keen, T. Ishii, B. Hirschberg, C. T. Bond, S. Lutsenko, J. Maylie, J. P. Adelman, Mechanism of calcium gating in small-conductance calcium-activated potassium channels. *Nature* **395**, 503–507 (1998).
14. M. Yu, J. C. Bean, H. Liu, Y. He, Y. Yang, X. Cai, K. Yu, Z. Pei, H. Liu, L. Tu, K. M. Conde, M. Wang, Y. Li, N. Yin, N. Zhang, J. Han, N. A. Scarcelli, P. Xu, Y. He, Y. Xu, C. Wang, SK3 in POMC neurons plays a sexually dimorphic role in energy and glucose homeostasis. *Cell Biosci.* **12**, 170 (2022).
15. M. Stocker, P. Pedarzani, Differential distribution of three Ca^{2+}-activated K^+ channel subunits, SK1, SK2, and SK3, in the adult rat central nervous system. *Mol. Cell. Neurosci.* **15**, 476–493 (2000).
16. F. E. Henry, K. Sugino, A. Tozer, T. Branco, S. M. Sternson, Cell type-specific transcriptomics of hypothalamic energy-sensing neuron responses to weight-loss. *eLife* **4**, e09800 (2015).
17. Y. He, G. Shu, Y. Yang, P. Xu, Y. Xia, C. Wang, K. Saito, A. Hinton Jr., X. Yan, C. Liu, Q. Wu, Q. Tong, Y. Xu, A small potassium current in AgRP/NPY neurons regulates feeding behavior and energy metabolism. *Cell Rep.* **17**, 1807–1818 (2016).
18. C. Yan, Y. He, Y. Xu, G. Shu, C. Wang, Y. Yang, K. Saito, P. Xu, A. O. Hinton Jr., X. Yan, L. Yu, Q. Wu, P. Tso, Q. Tong, Y. Xu, Apolipoprotein A-IV inhibits AgRP/NPY neurons and activates pro-opiomelanocortin neurons in the arcuate nucleus. *Neuroendocrinology* **103**, 476–488 (2016).
19. Y. He, P. Xu, C. Wang, Y. Xia, M. Yu, Y. Yang, K. Yu, X. Cai, N. Qu, K. Saito, J. Wang, I. Hyseni, M. Robertson, B. Piyarathna, M. Gao, S. A. Khan, F. Liu, R. Chen, C. Coarfa, Z. Zhao, Q. Tong, Z. Sun, Y. Xu, Estrogen receptor-α expressing neurons in the ventrolateral VMH regulate glucose balance. *Nat. Commun.* **11**, 2165 (2020).
20. A. C. Acara, M. Bolatkale, I. Kiziloglu, E. Ibisoglu, C. Can, A novel biochemical marker for predicting the severity of ACS with unstable angina pectoris: Asprosin. *Am. J. Emerg. Med.* **36**, 1504–1505 (2018).
21. M. M. Donma, O. Donma, Asprosin: Possible target in connection with ghrelin and cytokine network expression in the post-burn treatment. *Med. Hypotheses* **118**, 163–168 (2018).
22. X. Li, M. Liao, R. Shen, L. Zhang, H. Hu, J. Wu, X. Wang, H. Qu, S. Guo, M. Long, H. Zheng, Plasma asprosin levels are associated with glucose metabolism, lipid, and sex hormone profiles in females with metabolic-related diseases. *Mediators Inflamm.* **2018**, 7375294 (2018).
23. Y. Liu, A. Long, L. Chen, L. Jia, Y. Wang, The asprosin-OLFR734 module regulates appetitive behaviors. *Cell Discov.* **6**, 19 (2020).
24. M. Alan, B. Gurlek, A. Yilmaz, M. Aksit, B. Aslanipour, I. Gulhan, C. Mehmet, C. E. Taner, Asprosin: A novel peptide hormone related to insulin resistance in women with polycystic ovary syndrome. *Gynecol. Endocrinol.* **35**, 220–223 (2019).
25. J. B. Groener, A. Valkanou, Z. Kender, J. Pfeiffenberger, L. Kihm, T. Fleming, P. P. Nawroth, S. Kopf, Asprosin response in hypoglycemia is not related to hypoglycemia unawareness but rather to insulin resistance in type 1 diabetes. *PLOS ONE* **14**, e0222771 (2019).
26. T. Lee, S. Yun, J. H. Jeong, T. W. Jung, Asprosin impairs insulin secretion in response to glucose and viability through TLR4/JNK-mediated inflammation. *Mol. Cell. Endocrinol.* **486**, 96–104 (2019).
27. K. Ugur, S. Aydin, Saliva and blood asprosin hormone concentration associated with obesity. *Int. J. Endocrinol.* **2019**, 2521096 (2019).
28. C. Y. Wang, T. A. Lin, K. H. Liu, C. H. Liao, Y. Y. Liu, V. C. Wu, M. S. Wen, T. S. Yeh, Serum asprosin levels and bariatric surgery outcomes in obese adults. *Int. J. Obes.* **43**, 1019–1025 (2019).
29. X. Zhang, H. Jiang, X. Ma, H. Wu, Increased serum level and impaired response to glucose fluctuation of asprosin is associated with type 2 diabetes mellitus. *J. Diabetes Investig.* **11**, 349–355 (2020).
30. G. Eser Karlidag, O. Arslan Solmaz, Are adropin, apelin, elabela, asprosin and betatrophin biomarkers for chronic hepatitis and staging of fibrosis? *Biotech. Histochem.* **95**, 152–159 (2020).
31. C. Du, C. Wang, X. Guan, J. Li, X. Du, Z. Xu, B. Li, Y. Liu, F. Fu, H. Huo, Z. Zheng, Asprosin is associated with anorexia and body fat mass in cancer patients. *Support. Care Cancer* **29**, 1369–1375 (2021).
32. I. Mishra, C. Duerrschmid, Z. Ku, Y. He, W. Xie, E. S. Silva, J. Hoffman, W. Xin, N. Zhang, Y. Xu, Z. An, A. R. Chopra, Asprosin-neutralizing antibodies as a treatment for metabolic syndrome. *eLife* **10**, e63784 (2021).
33. K. F. Herrik, J. P. Redrobe, D. Holst, C. Hougaard, K. Sandager-Nielsen, A. N. Nielsen, H. Ji, N. M. Holst, H. B. Rasmussen, E. O. Nielsen, D. Strobaek, P. D. Shepard, P. Christophersen, CyPPA, a positive SK3/SK2 modulator, reduces activity of dopaminergic neurons, inhibits dopamine release, and counteracts hyperdopaminergic behaviors induced by methylphenidate. *Front. Pharmacol.* **3**, 11 (2012).
34. D. I. Briggs, P. J. Enriori, M. B. Lemus, M. A. Cowley, Z. B. Andrews, Diet-induced obesity causes ghrelin resistance in arcuate NPY/AgRP neurons. *Endocrinology* **151**, 4745–4755 (2010).
35. Q. Wang, C. Liu, A. Uchida, J. C. Chuang, A. Walker, T. Liu, S. Osborne-Lawrence, B. L. Mason, C. Mosher, E. D. Berglund, J. K. Elmquist, J. M. Zigman, Arcuate AgRP neurons mediate orexigenic and glucoregulatory actions of ghrelin. *Mol. Metab.* **3**, 64–72 (2014).
36. R. M. de Guia, A. S. Hassing, T. Ma, K. Plucinska, B. Holst, Z. Gerhart-Hines, B. Emanuelli, J. T. Treebak, Ablation of Nampt in AgRP neurons leads to neurodegeneration and impairs fasting- and ghrelin-mediated food intake. *FASEB J.* **35**, e21450 (2021).
37. D. B. Glass, H. C. Cheng, L. Mende-Mueller, J. Reed, D. A. Walsh, Primary structural determinants essential for potent inhibition of cAMP-dependent protein kinase by inhibitory peptides corresponding to the active portion of the heat-stable inhibitor protein. *J. Biol. Chem.* **264**, 8802–8810 (1989).
38. H. B. Ruan, M. O. Dietrich, Z. W. Liu, M. R. Zimmer, M. D. Li, J. P. Singh, K. Zhang, R. Yin, J. Wu, T. L. Horvath, X. Yang, O-GlcNAc transferase enables AgRP neurons to suppress browning of white fat. *Cell* **159**, 306–317 (2014).

39. Y. W. Nam, D. Kong, D. Wang, R. Orfali, R. T. Sherpa, J. Totonchy, S. M. Nauli, M. Zhang, Differential modulation of SK channel subtypes by phosphorylation. *Cell Calcium* **94**, 102346 (2021).
40. F. Vogalis, J. R. Harvey, J. B. Furness, PKA-mediated inhibition of a novel K^+ channel underlies the slow after-hyperpolarization in enteric AH neurons. *J. Physiol.* **548**, 801–814 (2003).
41. Y. Ren, L. F. Barnwell, J. C. Alexander, F. D. Lubin, J. P. Adelman, P. J. Pfaffinger, L. A. Schrader, A. E. Anderson, Regulation of surface localization of the small conductance Ca^{2+}-activated potassium channel, Sk2, through direct phosphorylation by cAMP-dependent protein kinase. *J. Biol. Chem.* **281**, 11769–11779 (2006).
42. M. T. Lin, R. Lujan, M. Watanabe, J. P. Adelman, J. Maylie, SK2 channel plasticity contributes to LTP at Schaffer collateral-CA1 synapses. *Nat. Neurosci.* **11**, 170–177 (2008).
43. A. Belmeguenai, E. Hosy, F. Bengtsson, C. M. Pedroarena, C. Piochon, E. Teuling, Q. He, G. Ohtsuki, M. T. De Jeu, Y. Elgersma, C. I. De Zeeuw, H. Jorntell, C. Hansel, Intrinsic plasticity complements long-term potentiation in parallel fiber input gain control in cerebellar Purkinje cells. *J. Neurosci.* **30**, 13630–13643 (2010).
44. K. Abiraman, M. Sah, R. S. Walikonis, G. Lykotrafitis, A. V. Tzingounis, Tonic PKA activity regulates SK channel nanoclustering and somatodendritic distribution. *J. Mol. Biol.* **428**, 2521–2537 (2016).
45. C. Ballesteros-Merino, M. Lin, W. W. Wu, C. Ferrandiz-Huertas, M. J. Cabanero, M. Watanabe, Y. Fukazawa, R. Shigemoto, J. Maylie, J. P. Adelman, R. Lujan, Developmental profile of SK2 channel expression and function in CA1 neurons. *Hippocampus* **22**, 1467–1480 (2012).
46. C. A. Sailer, H. Hu, W. A. Kaufmann, M. Trieb, C. Schwarzer, J. F. Storm, H. G. Knaus, Regional differences in distribution and functional expression of small-conductance Ca^{2+}-activated K^+ channels in rat brain. *J. Neurosci.* **22**, 9698–9707 (2002).
47. S. E. Bowden, S. Fletcher, D. J. Loane, N. V. Marrion, Somatic colocalization of rat SK1 and D class ($Ca_v1.2$) L-type calcium channels in rat CA1 hippocampal pyramidal neurons. *J. Neurosci.* **21**, –RC175 (2001).
48. C. Ballesteros-Merino, M. Watanabe, R. Shigemoto, Y. Fukazawa, J. P. Adelman, R. Lujan, Differential subcellular localization of SK3-containing channels in the hippocampus. *Eur. J. Neurosci.* **39**, 883–892 (2014).
49. Y. Ni, T. Wang, X. Zhuo, B. Song, J. Zhang, F. Wei, H. Bai, X. Wang, D. Yang, L. Gao, A. Ma, Bisoprolol reversed small conductance calcium-activated potassium channel (SK) remodeling in a volume-overload rat model. *Mol. Cell. Biochem.* **384**, 95–103 (2013).
50. T. Y. Kim, R. Terentyeva, K. H. Roder, W. Li, M. Liu, I. Greener, S. Hamilton, I. Polina, K. R. Murphy, R. T. Clements, S. C. Dudley Jr., G. Koren, B. R. Choi, D. Terentyev, SK channel enhancers attenuate Ca^{2+}-dependent arrhythmia in hypertrophic hearts by regulating mito-ROS-dependent oxidation and activity of RyR. *Cardiovasc. Res.* **113**, 343–353 (2017).
51. Y. Chen, Y. C. Lin, T. W. Kuo, Z. A. Knight, Sensory detection of food rapidly modulates arcuate feeding circuits. *Cell* **160**, 829–841 (2015).
52. Y. Yang, D. Atasoy, H. H. Su, S. M. Sternson, Hunger states switch a flip-flop memory circuit via a synaptic AMPK-dependent positive feedback loop. *Cell* **146**, 992–1003 (2011).
53. M. Koch, Cannabinoid receptor signaling in central regulation of feeding behavior: A mini-review. *Front. Neurosci.* **11**, 293 (2017).
54. K. Sureshkumar, A. Saenz, S. M. Ahmad, K. Lutfy, The PACAP/PAC1 receptor system and feeding. *Brain Sci.* **12**, 13 (2021).
55. X. Fioramonti, N. Marsollier, Z. Song, K. A. Fakira, R. M. Patel, S. Brown, T. Duparc, A. Pica-Mendez, N. M. Sanders, C. Knauf, P. Valet, R. J. McCrimmon, A. Beuve, C. Magnan, V. H. Routh, Ventromedial hypothalamic nitric oxide production is necessary for hypoglycemia detection and counterregulation. *Diabetes* **59**, 519–528 (2010).
56. B. A. Murphy, K. A. Fakira, Z. Song, A. Beuve, V. H. Routh, AMP-activated protein kinase and nitric oxide regulate the glucose sensitivity of ventromedial hypothalamic glucose-inhibited neurons. *Am. J. Physiol. Cell Physiol.* **297**, C750–C758 (2009).
57. C. Wang, E. Bomberg, C. J. Billington, A. S. Levine, C. M. Kotz, Brain-derived neurotrophic factor (BDNF) in the hypothalamic ventromedial nucleus increases energy expenditure. *Brain Res.* **1336**, 66–77 (2010).
58. Z. Wu, E. R. Kim, H. Sun, Y. Xu, L. R. Mangieri, D. P. Li, H. L. Pan, Y. Xu, B. R. Arenkiel, Q. Tong, GABAergic projections from lateral hypothalamus to paraventricular hypothalamic nucleus promote feeding. *J. Neurosci.* **35**, 3312–3318 (2015).
59. X. Zhang, A. N. van den Pol, Rapid binge-like eating and body weight gain driven by zona incerta GABA neuron activation. *Science* **356**, 853–859 (2017).
60. J. Deignan, R. Lujan, C. Bond, A. Riegel, M. Watanabe, J. T. Williams, J. Maylie, J. P. Adelman, SK2 and SK3 expression differentially affect firing frequency and precision in dopamine neurons. *Neuroscience* **217**, 67–76 (2012).
61. E. K. Brinkman, T. Chen, M. Amendola, B. van Steensel, Easy quantitative assessment of genome editing by sequence trace decomposition. *Nucleic Acids Res.* **42**, e168 (2014).
62. M. S. Gold, M. J. Shuster, J. D. Levine, Role of a Ca^{2+}-dependent slow afterhyperpolarization in prostaglandin E_2-induced sensitization of cultured rat sensory neurons. *Neurosci. Lett.* **205**, 161–164 (1996).
63. P. Pagadala, C. K. Park, S. Bang, Z. Z. Xu, R. G. Xie, T. Liu, B. X. Han, W. D. Tracey Jr., F. Wang, R. R. Ji, Loss of NR1 subunit of NMDARs in primary sensory neurons leads to hyperexcitability and pain hypersensitivity: Involvement of Ca^{2+}-activated small conductance potassium channels. *J. Neurosci.* **33**, 13425–13430 (2013).
64. X. Cao, P. Xu, M. G. Oyola, Y. Xia, X. Yan, K. Saito, F. Zou, C. Wang, Y. Yang, A. Hinton Jr., C. Yan, H. Ding, L. Zhu, L. Yu, B. Yang, Y. Feng, D. J. Clegg, S. Khan, R. DiMarchi, S. K. Mani, Q. Tong, Y. Xu, Estrogens stimulate serotonin neurons to inhibit binge-like eating in mice. *J. Clin. Invest.* **124**, 4351–4362 (2014).
65. G. Y. Zan, Y. J. Wang, X. P. Li, J. F. Fang, S. Y. Yao, J. Y. Du, Q. Wang, X. Sun, R. Liu, X. M. Shao, J. D. Long, J. R. Chai, Y. Z. Deng, Y. Q. Chen, Q. L. Li, J. Q. Fang, Z. Q. Liu, J. G. Liu, Amygdalar κ-opioid receptor-dependent upregulating glutamate transporter 1 mediates depressive-like behaviors of opioid abstinence. *Cell Rep.* **37**, 109913 (2021).
66. Y. D. Li, Y. J. Luo, Z. K. Chen, L. Quintanilla, Y. Cherasse, L. Zhang, M. Lazarus, Z. L. Huang, J. Song, Hypothalamic modulation of adult hippocampal neurogenesis in mice confers activity-dependent regulation of memory and anxiety-like behavior. *Nat. Neurosci.* **25**, 630–645 (2022).
67. T. Ni, L. Zhu, S. Wang, W. Zhu, Y. Xue, Y. Zhu, D. Ma, H. Wang, F. Guan, T. Chen, Medial prefrontal cortex Notch1 signalling mediates methamphetamine-induced psychosis via Hes1-dependent suppression of GABAB1 receptor expression. *Mol. Psychiatry* **27**, 4009–4022 (2022).

Acknowledgments: We thank the Laboratory of Animal Center of Pennington Biomedical Research Center at Louisiana State University, Baylor College of Medicine, and Case Western Reserve University for invaluable help in mouse colony maintenance. We acknowledge J. K. Elmquist and C. Liu for providing AgRP-CreERT2 transgenic mice. We acknowledge A. Chopra for providing *Ptprd*$^{f/f}$ mice. We acknowledge Y. Xu and A. Chopra for comments on this manuscript. **Funding:** This work was supported by grants from the NIH (R01 DK123098 and P30 DK020595 to P.X.; P20 GM135002 and R01 DK129548 to Y.H.; and K01DK119471 to C.W.), DOD (Innovative Grant W81XWH-20-1-0075 to P.X.), American Heart Association award (19CDA34660335 to C.W.), American Diabetes Association postdoctoral fellowship award (1-17-PDF-138 to Y.H.), and USDA/CRIS [3092-51000-062-04(B)S to C.W.]. **Author contributions:** B.F., H.L., and I.M. are the main contributors to the conduct of the study, data collection, and data analysis. C.D. and P.G. contributed to the conduct of the study. P.X., C.W., and Y.H. contributed to the study design, data interpretation, and manuscript writing. **Competing interests:** The authors declare that they have no competing interests. **Data and materials availability:** All data needed to evaluate the conclusions in the paper are present in the paper and/or the Supplementary Materials.

Submitted 1 May 2022
Accepted 20 January 2023
Published 22 February 2023
10.1126/sciadv.abq6718